New heterobimetallic ferrocenyl derivatives are promising antitrypanosomal agents

Esteban Rodríguez Arce[a], Eugenia Putzu[a], Michel Lapier[b], Juan Diego Maya[c], Claudio Olea Azar[b], Gustavo A. Echeverría[d], Oscar E. Piro[d], Andrea Medeiros[e,f], Florencia Sardi[e], Marcelo Comini[e], Gastón Risi[g], Gustavo Salinas [g], Isabel Correia,[h] João Costa Pessoa,[h] Lucía Otero[a*], Dinorah Gambino[a*]

[a] Química Inorgánica, Facultad de Química, Universidad de la República, Gral. Flores 2124, 11800 Montevideo, Uruguay.

[b] Departamento de Química Inorgánica y Analítica, Facultad de Ciencias Químicas y Farmacéuticas, Universidad de Chile, Casilla 233, Santiago, Chile.

[c] ICBM, Facultad de Medicina, Universidad de Chile, Av. Independencia 1027, Santiago, Chile.

[d] Departamento de Física, Facultad de Ciencias Exactas, Universidad Nacional de La Plata and Institut IFLP (CONICET, CCT-La Plata), C.C. 67, 1900 La Plata, Argentina.

[e] Group Redox Biology of Trypanosomes, Institut Pasteur de Montevideo, Mataojo 2020, CP 11400, Montevideo, Uruguay

[f] Departamento de Bioquímica, Facultad de Medicina, Universidad de la República, Gral. Flores 2125, 11800 Montevideo, Uruguay.

[g] Worm Biology Lab, Institut Pasteur de Montevideo, Montevideo, Uruguay.

[h] Centro de Química Estrutural, Instituto Superior Técnico, Universidade de Lisboa, 1049-001 Lisboa, Portugal

* To whom correspondence should be addressed. E-mail: dgambino@fq.edu.uy; luotero@fq.edu.uy Tel. +5982-9249739; fax: +5982-9241906

Dalton Transactions Accepted Manuscript

Abstract

In the search for a more effective chemotherapy for the treatment of Chagas disease and Human African trypanosomiasis, caused by *Trypanosoma cruzi* and *Trypanosoma brucei* parasites, respectively, the use of organometallic compounds may be a promising strategy. In this work, eight new heterobimetallic compounds are described including four 5-nitrofuryl containing thiosemicarbazones as bioactive ligands (H**L1**-H**L4**) and dppf = 1,1'-bis(diphenylphosphino) ferrocene as organometallic co-ligand. Complexes of the formula [M^{II}(**L**)(dppf)](PF_6) with M = Pd or Pt were synthesized and fully characterized in the solid state and in solution, including the determination of the molecular structure of four of them by single crystal X-ray diffraction methods. Most compounds showed activity in the low micromolar or submicromolar range against both parasites, with the platinum compounds being more active than the palladium analogues. Activity was significantly increased by generation of the M-dppf compounds (3-24 fold increase in respect to free ligands HL for *T. cruzi* and up to 99 fold increase in respect to HL for *T. brucei*). The inclusion of the organometallic co-ligand also led to lower toxicity on mammalian cells and higher selectivity towards both parasites when compared to the free HL compounds. The complexes interact with DNA and affect the redox metabolism of the parasites. Furthermore, the most active and selective compound of the new series, showed no *in vivo* toxicity on zebrafish embryos.

Introduction

Infectious diseases represent a tremendous health burden worldwide. Among them, a group of seventeen communicable and poverty-related diseases, that affect about one billion people living in 149 countries, have received scarce attention from the pharmaceutical industry, probably due to low prospect of generating financial profit. These illnesses are therefore

considered as neglected diseases by the World Health Organization. Our research group has

focused its interest on two neglected parasitic diseases: American Trypanosomiasis (Chagas´

disease) and Human African Trypanosomiasis (sleeping sickness). These diseases are caused

by the genetically related trypanosomatid parasites *Trypanosoma cruzi* and *Trypanosoma*

brucei which share a high percentage of conserved genes. This fact offers the opportunity to

develop wide spectrum drugs that might affect both parasites, leading to drugs suitable for

the treatment of both diseases.[1-3]

Chagas' disease is an ancient and endemic illness in Latin America caused by the flagellated

protozoan parasite *Trypanosoma cruzi* (*T. cruzi*). It is mainly transmitted to the mammalian

host by infected blood-sucking triatomine bugs. In Latin America and the Caribbean region,

the burden of the disease is five times greater than that of malaria. Intense migration flow

towards the United States, Australia, Europe and Japan, has led, in the last decades, to an

increase in the number of cases in these non-endemic regions due to other non-bug

associated transmission ways, like blood transfusions, organ transplants and transmission

from mother to newborn. [4-6]

Human African trypanosomiasis (HAT) or sleeping sickness is caused by two subspecies of

Trypanosoma brucei (*T. brucei*): *Trypanosoma brucei gambiense* and *Trypanosoma brucei*

rhodesiense. It is transmitted by the bite of a tsetse fly. It is restricted to poor regions of

Africa affecting mainly people living in rural areas. *T. brucei rhodesiense* causes the most

virulent form of the disease being usually fatal if left untreated. The animal disease, called

Nagana, is also threatening since it severely affects domestic animals within the rural areas.

[7,8]

New drugs are urgently needed for the treatment of both diseases. Current chemotherapy is

quite old and suffers from several drawbacks. The most widely used drugs are Nifurtimox

and Benznidazole for Chagas disease and Melarsoprol B and Eflornithine for HAT. They all

show high toxicity and severe side effects, variable results associated with strain-specific differences in susceptibility and drug resistance. Additionally, prolonged treatment regimens are required.[6,8]

The development of metal-based drugs has shown to be a promising approach in the search for pharmacological answers to parasitic diseases. Prospective metal-based drugs against highly prevalent parasitic illnesses have been identified. Among them, some ferrocenyl derivatives and other organometallics have shown promising results. [9-16] In this context, our main design strategy has been to develop metal compounds with known bioactive molecules as ligands, particularly bioactive 5-nitrofuryl containing thiosemicarbazones (Fig. 1). These compounds, containing the 5-nitrofurane pharmacophore moiety, were obtained as analogs of the reference antitrypanosomal drug Nifurtimox. Although they showed very good activities *in vitro* against *T. cruzi*, they were also rather toxic against mammalian cells.[17] The mechanism of action of these compounds includes the reduction of the nitro group to a nitro anion by parasite enzymes generating free radical species (ROS) that are very toxic to *T. cruzi*.[17] In order to improve the pharmacological properties of these organic compounds and to modulate biologically relevant physicochemical properties of their metal complexes, more than eighty classical and organometallic compounds have been developed till now. Metal compounds were rationally designed by modifying the metal center and the metal ion oxidation state and including different organometallic cores and different co-ligands.[9]

On the other hand, in the search for new drugs against trypanosomatid parasites we successfully developed some very interesting ferrocenyl prospective anti-*T. cruzi* drugs including the bioactive ligand pyridine-2-thiolato-1-oxide. [18]

All these antecedents prompted us to develop a new family of palladium and platinum compounds with 5-nitrofuryl containing thiosemicarbazones as ligands and including an organometallic ferrocenyl moiety (Fig. 1). Palladium and platinum were selected based on

our previous promising results as well as the proved importance of these metal ions in the

medicinal chemistry field [14,18,19] In this work, eight 1,1'-bis(diphenylphosphino) ferrocene

(dppf) compounds, $[M^{II}(L)(dppf)](PF_6)$, where M = palladium or platinum and H**L** = 5-

nitrofuryl thiosemicarbazones H**L1**-H**L4** (Fig. 1), were synthesized and fully characterized in

the solid state and in solution. The new compounds were evaluated on *T. cruzi*

trypomastigotes and bloodstream *T. brucei* as well as on endothelial mammalian cells taken

as mammalian cell model. The toxicity of the most active and selective compound of the

series was also evaluated *in vivo* on zebrafish embryos. To get insight into the probable

mechanism of action of the new compounds, interaction with biomolecules and generation of

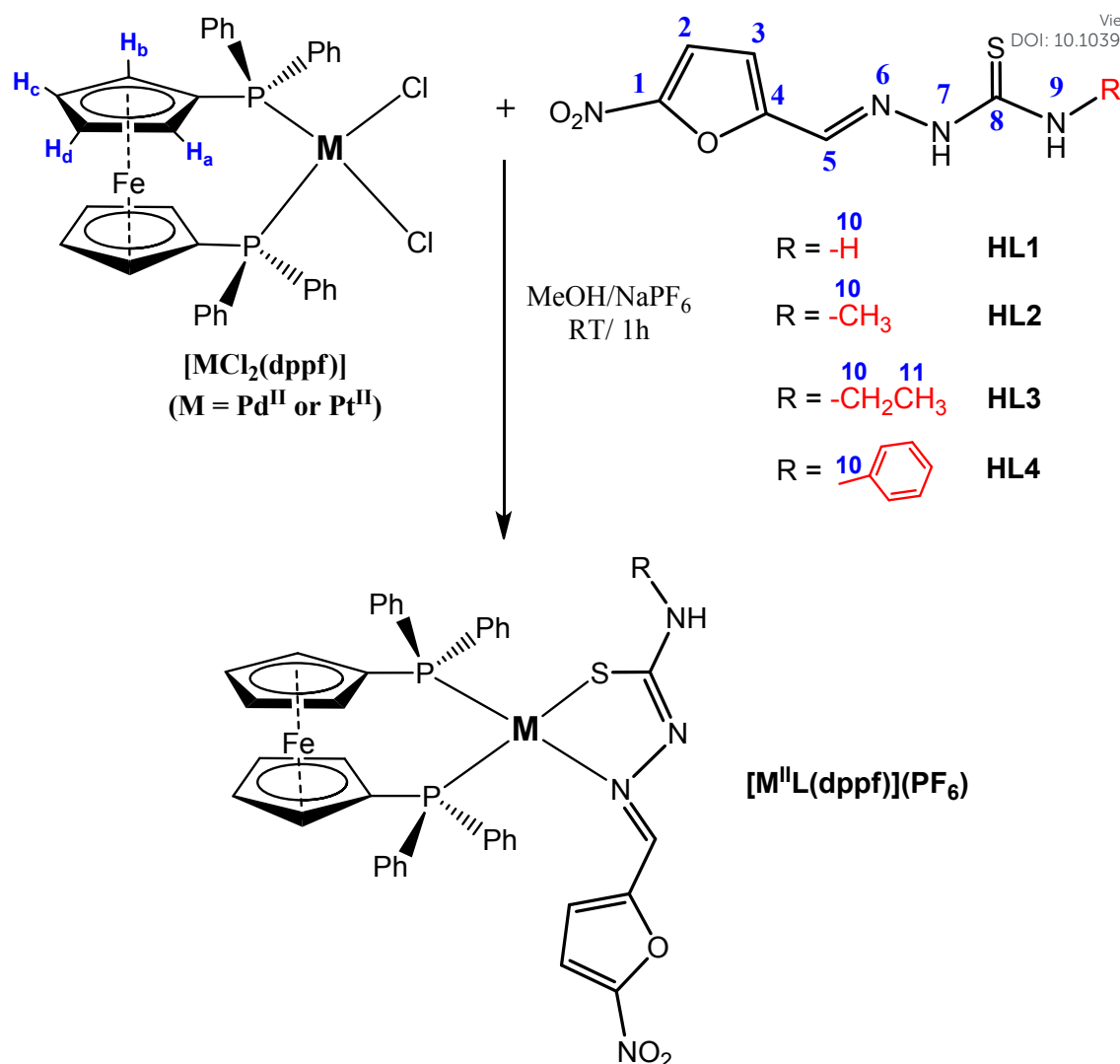intra-parasite ROS were also studied.

Fig. 1. Scheme of synthesis of the new $[M^{II}(L)(dppf)](PF_6)$ complexes, where M = Pd

or Pt and H**L1**-H**L4** = 5-nitrofuryl containing thiosemicarbazones.

Experimental section

General considerations

All common laboratory chemicals were purchased from commercial sources and used

without further purification. The thiosemicarbazone ligands H**L** were prepared as previously

reported.[17] [MCl₂(dppf)] precursors were synthesized according to a previously reported

procedure by heating for 30 min an equimolar mixture of $[MCl_2(dmso)_2]$ and dppf in

$CHCl_3$.[20]

Chemical and Physical Measurements

C, H and N analyses were performed with a Thermo Scientific Flash 2000 elemental

analyzer. FTIR spectra (4000 - 400 cm^{-1}) of the complexes and the H**L** compounds were

measured as KBr pellets with a Shimadzu IR Prestige-21 instrument. Conductimetric

measurements were done over time (5 days) at 25 ℃ in 10^{-3} M DMSO solutions using a

Conductivity Meter 4310 Jenway to determine the type of electrolyte and to assess the

stability of the complexes in such medium.[21] ^{1}H NMR and ^{13}C NMR spectra were recorded

in DMSO-d_6 at 30 ℃ on a Bruker DPX-400 instrument (at 400 MHz and 100 MHz,

respectively). Homo-nuclear (COSY) and hetero-nuclear (2D-HETCOR) correlation

experiments (HSQC: hetero-nuclear single quantum correlation and HMBC: hetero-nuclear

multiple bond correlation) were carried out with the same instrument. Tetramethylsilane was

used as the internal standard and chemical shifts are reported in ppm. A LCQ Fleet™ Ion

Trap Mass Spectrometer from Thermo Scientific was used to measure ESI-MS spectra of

methanolic solutions of the complexes in the positive and negatives modes. Cyclic

voltammograms were obtained with an Epsilon Electrochemical Analyzer. A glassy carbon

electrode was employed as working electrode, a platinum wire was used as counter electrode

while a Ag/AgCl electrode was used as reference electrode. A standard electrochemical three

electrode cell of 10 mL volume completed the system. Measurements were carried out at

room temperature in 1 mM acetonitrile solutions of the compounds using tetrabutyl amonium

hexafluorophosphate (*ca.* 0.1 M) as supporting electrolyte. Solutions were deoxygenated *via*

purging with nitrogen for 15 min, prior to the measurements.

Syntheses of [M(L)(dppf)](PF$_6$), where M = Pd(II) or Pt(II) and HL = 5-nitrofuryl containing thiosemicarbazones HL1-HL4

The heterobimetallic compounds were synthesized by the following procedure: 50 mg of the precursor [MCl$_2$(dppf)]·CHCl$_3$ (0.059 mmol [PdCl$_2$(dppf)]·CHCl$_3$ or 0.053 mmol [PtCl$_2$(dppf)]·CHCl$_3$) were dissolved in 10 mL methanol. To this solution, an equimolar amount of HL (13 mg HL1, 13 mg HL2, 14 mg HL3 and 17 mg HL4 for the Pd compounds and 11 mg HL1, 12 mg HL2, 13 mg HL3 and 15 mg HL4 for the Pt compounds) dissolved in 5 mL methanol was added. The mixture was stirred at room temperature for 1 h. The solution volume was reduced to 5 mL and then kept in the refrigerator. After adding NaPF$_6$ dissolved in a minimal volume of methanol (46 mg, 0.27 mmol) the solution was kept again in the refrigerator during 24 h. Pd compounds were isolated as brown solids and the Pt analogues as orange-yellow ones. The eight compounds were recrystallized from dichloromethane solutions of the compounds by adding hexane.

***[PdL1(dppf)](PF$_6$)·CH$_2$Cl$_2$,* Pd-dppf-L1** Yield: 40 mg, 61%. Found: C, 44.52; H, 3.30; N, 5.08. Calc. for C$_{41}$H$_{35}$Cl$_2$F$_6$FeN$_4$O$_3$P$_3$PdS: C, 44.62; H, 3.20; N, 5.08. ESI MS *m/z*: [Calculated (Found)]: 873.01 (873.18) [PdL1(dppf)]$^+$, 100%; 144.96 (144.82) PF$_6^-$, 100%. FTIR (KBr, cm^{-1}): 1605, ν(C = N); 1353, ν_s(NO$_2$); 1098, ν(N-N); 810, δ(NO$_2$ + furan); 842, ν(P-F); 558, δ(FPF); 1480, 1437, 1090, 698, 493, dppf. ^{1}H NMR [DMSO-d_6, Me$_4$Si, δ/ppm]: 7.91 [m, 5, H2 + PPh$_2$], 7.81 [m, 1, H3], 7.76 [m, 5, H9 + H10 + PPh$_2$], 7.62 [m, 9, PPh$_2$], 7.46 [m, 4, PPh$_2$], 6.61 [s, 1 H5], 4.88 [s, 2, H$_c$], 4.77 [s, 2, H$_b$], 4.62 [s, 2, H$_a$], 3.86 [s, 2, H$_d$]. ^{13}C NMR [DMSO-d_6, δ/ppm]: 174.9 (C8), 140.1

(C5), 135.1 (C2), 134.9 (C3), 134.7 (CH, PPh$_2$), 134.2 (C10), 129.9 (CH, PPh$_2$), 129.0 (CH, PPh$_2$), 123.1 (CH, PPh$_2$), 77.8 (C$_c$), 75.8 (C$_d$), 75.2 (C$_b$), 75.1 (C$_a$).

[PdL2(dppf)](PF$_6$)·2CH$_2$Cl$_2$, Pd-dppf-L2 Yield: 44 mg, 62%. Found: C, 42.15; H, 3.34; N, 4.73. Calc. for C$_{43}$H$_{39}$Cl$_4$F$_6$FeN$_4$O$_3$P$_3$PdS: C, 42.14; H, 3.27; N, 4.66. ESI MS *m/z*: [Calculated (Found)]: 887.03 (887.21) [PdL2(dppf)]$^+$, 100%; 144.96 (144.84) PF$_6^-$, 100%. FTIR (KBr, cm^{-1}): 1591, ν(C = N); 1350, ν_s(NO$_2$); 1097, ν(N-N); 810, δ(NO$_2$ + furan); 844, ν(P-F); 557, δ(FPF); 1479, 1437, 1096, 696, 494, dppf. ^{1}H NMR [DMSO-d_6, Me$_4$Si, δ/ppm]: 8.23 [s, 1, H9], 7.94 [dd, J$_1$ = 7.80 Hz and J$_2$ = 3.80 Hz, 4, PPh$_2$], 7.77 [m, 4, PPh$_2$], 7.63 [m, 9, H2 + PPh$_2$], 7.47 [m, 4, PPh$_2$], 7.40 [d, J = 7.54 Hz, 1, H3], 6.67 [s, 1 H5], 4.85 [s, 2, H$_c$], 4.79 [s, 2, H$_b$], 4.63 [s, 2, H$_a$], 3.89 [s, 2, H$_d$], 3.83 [s, 3, H10]. ^{13}C NMR [DMSO-d_6, δ/ppm]: 174.5 (C8), 141.0 (C5), 135.0 (CH, PPh$_2$), 134.2 (CH, PPh$_2$), 133.1 (C2), 132.9 (CH, PPh$_2$), 129.1 (CH, PPh$_2$), 122.7 (C3), 78.0 (C$_c$), 75.8 (C$_d$), 75.7 (C$_b$), 75.1 (C$_a$), 33.6 (C10).

[PdL3(dppf)](PF$_6$)·2CH$_2$Cl$_2$, Pd-dppf-L3 Yield: 46 mg, 64%. Found: C, 43.86; H, 3.42; N, 4.40. Calc. For C$_{44}$H$_{41}$Cl$_4$F$_6$FeN$_4$O$_3$P$_3$PdS: C, 43.44; H, 3.40; N, 4.50. ESI MS *m/z*: [Calculated (Found)]: 901.04 (901.21) [PdL3(dppf)]$^+$, 100%; 144.96 (144.83) PF$_6^-$, 100%. FTIR (KBr, cm^{-1}): 1591, ν(C = N); 1345, ν_s(NO$_2$); 1098, ν(N-N); 811, δ(NO$_2$ + furan); 853, ν(P-F); 557, δ(FPF); 1471, 1437, 1097, 694, 500, dppf. ^{1}H NMR [DMSO-d_6, Me$_4$Si, δ/ppm]: 8.22 [s, 1, H9], 7.91 [dd, J$_1$ = 7.10 Hz and J$_2$ = 3.09 Hz, 4, PPh$_2$], 7.76 [m, 4, PPh$_2$], 7.63 [m, 9, H2 + PPh$_2$], 7.47 [m, 4, PPh$_2$], 7.36 [d, J = 6.76 Hz, 1, H3], 6.73 [s, 1, H5], 4.81 [s, 2, H$_c$], 4.77 [s, 2, H$_b$], 4.64 [s, 2, H$_a$], 3.94 [s, 2, H$_d$], 1.11 [t, J = 6.40 Hz, 3, H11]. ^{13}C NMR [DMSO-d_6, δ/ppm]: 174.5 (C8), 143.2 (C5), 135.1 (CH, PPh$_2$), 134.3 (CH, PPh$_2$), 133.1 (CH, PPh$_2$), 132.8 (C2), 129.0 (CH, PPh$_2$), 128.9 (C3), 77.9 (C$_c$), 77.6 (C$_b$), 76.4 (C$_d$), 74.9 (C$_a$), 14.3 (C11).

[PdL4(dppf)](PF$_6$)·1.5CH$_2$Cl$_2$, **Pd-dppf-L4** Yield: 50 mg, 71%. Found: C, 47.03; H, 3.29; N, 4.51. Calc. for C$_{47.5}$H$_{40}$Cl$_3$F$_6$FeN$_4$O$_3$P$_3$PdS: C, 46.68; H, 3.28; N, 4.58. ESI MS *m/z*: [Calculated (Found)]: 949.04 (949.21) [PdL4(dppf)]$^+$, 100%; 144.96 (144.87) PF$_6^-$, 100%. FTIR (KBr, cm^{-1}): 1598, ν(C = N); 1348, ν$_s$(NO$_2$); 1097, ν(N-N); 812, δ(NO$_2$ + furan); 845, ν(P-F); 558, δ(FPF); 1480, 1438, 1099, 692, 492, dppf. ^{1}H NMR [DMSO-*d*$_6$, Me$_4$Si, δ/ppm]: 10.19 [s, 1, H9], 7.93 [m, 4, PPh$_2$], 7.82 [m, 4, PPh$_2$], 7.65 [m, 5, H2 + PPh$_2$], 7.55 [m, 8, PPh$_2$], 7.42 [m, 2, H$_{orto}$], 7.34 [m, 3, H3 + H$_{meta}$], 7.12 [t, J = 7.31 Hz, 1, H$_{para}$], 6.74 [s, 1, H5], 4.76 [s, 2, H$_b$], 4.69 [s, 4, H$_a$ + H$_c$], 4.16 [s, 2, H$_d$]. ^{13}C NMR [DMSO-*d*$_6$, δ/ppm]: 173.2 (C8), 142.7 (C5), 135.4 (CH, PPh$_2$), 134.4 (CH, PPh$_2$), 133.0 (C2), 133.0 (CH, PPh$_2$), 129.8 (CH, PPh$_2$), 129.3 (C$_{meta}$), 128.7 (C3), 124.8 (C$_{para}$), 121.5 (C$_{orto}$), 77.6 (C$_c$), 76.3 (C$_d$), 75.1 (C$_a$), 74.4 (C$_b$).

[PtL1(dppf)](PF$_6$)·2CH$_2$Cl$_2$, **Pt-dppf-L1** Yield: 47 mg, 70%. Found: C, 40.08; H, 3.02; N, 4.41. Calc. for C$_{42}$H$_{37}$Cl$_4$F$_6$FeN$_4$O$_3$P$_3$PtS: C, 39.50; H, 2.90; N, 4.39. ESI MS *m/z*: [Calculated (Found)]: 962.07 (962.22) [PtL1(dppf)]$^+$, 100%; 144.96 (144.87) PF$_6^-$, 100%. FTIR (KBr, cm^{-1}): 1608, ν(C = N); 1346, ν$_s$(NO$_2$); 1098, ν(N-N); 810, δ(NO$_2$ + furan); 841, ν(P-F); 558, δ(FPF); 1480, 1437, 1099, 695, 498, dppf. ^{1}H NMR [DMSO-*d*$_6$, Me$_4$Si, δ/ppm]: 8.13 [s, br, H9 + H10], 7.95 [m, 4, PPh$_2$], 7.87 [d, J = 4.20 Hz, 1, H2], 7.77 [m, 1, H3], 7.75 [m, 4, PPh$_2$], 7.62 [m, 8, PPh$_2$], 7.47 [m, 4, PPh$_2$], 6.93 [s, 1, H5], 4.76 [s, 4, H$_b$ + H$_c$], 4.60 [s, 2, H$_d$], 3.90 [s, 2, H$_a$]. ^{13}C NMR [DMSO-*d*$_6$, δ/ppm]: 176.4 (C8), 141.8 (C5), 135.1 (CH, PPh$_2$), 135.1 (C2), 134.8 (C3), 134.2 (CH, PPh$_2$), 133.0 (C10), 129.3 (CH, PPh$_2$), 129.1 (CH, PPh$_2$), 77.2 (C$_c$), 76.3 (C$_a$), 75.7 (C$_b$), 74.9 (C$_d$).

[PtL2(dppf)](PF$_6$)·2CH$_2$Cl$_2$, **Pt-dppf-L2** Yield: 46 mg, 68%. Found: C, 40.00; H, 3.19; N, 4.36. Calc. for C$_{43}$H$_{39}$Cl$_4$F$_6$FeN$_4$O$_3$P$_3$PtS: C, 39.99; H, 3.03; N, 4.34. ESI MS *m/z*: [Calculated (Found)]: 976.9 (976.29) [PtL2(dppf)]$^+$, 100%; 144.96 (144.82) PF$_6^-$, 100%. FTIR (KBr, cm^{-1}): 1592, ν(C = N); 1349, ν$_s$(NO$_2$); 1094, ν(N-N); 812, δ(NO$_2$ + furan); 849,

Dalton Transactions

ν(P-F); 558, δ(FPF); 1479, 1437, 1096, 693, 495, dppf. ^{1}H NMR [DMSO-d_6, Me$_4$Si, δ/ppm]: 8.44 [s, 1, H9], 7.94 [dd, J_1 = 7.37 Hz and J_2 = 3.43 Hz, 4, PPh$_2$], 7.75 [m, 4, PPh$_2$], 7.62 [m, 9, H2 + PPh$_2$], 7.47 [m, 5, H3 + PPh$_2$], 7.06 [s, 1, H5], 4.75 [s, 2, H$_c$], 4.71 [s, 2, H$_b$], 4.64 [s, 2, H$_a$], 3.97 [s, 2, H$_d$], 2.87 [s, 3, H10]. ^{13}C NMR [DMSO-d_6, δ/ppm]: 177.7 (C8), 142.7 (C5), 135.2 (CH, PPh$_2$), 134.3 (CH, PPh$_2$), 133.1 (C2), 129.7 (CH, PPh$_2$), 129.1 (CH, PPh$_2$), 129.1 (C3), 77.0 (C$_b$), 76.0 (C$_d$), 75.4 (C$_c$), 75.0 (C$_a$), 34.1 (C10).

[PtL3(dppf)](PF$_6$)·CH$_2$Cl$_2$, Pt-dppf-L3 Yield: 47 mg, 72%. Found: C, 41.96; H, 3.25; N, 4.59. Calc. for C$_{43}$H$_{39}$Cl$_2$F$_6$FeN$_4$O$_3$P$_3$PtS: C, 42.32; H, 3.20; N, 4.59. ESI MS *m/z*: [Calculated (Found)]: 990.11 (990.29) [PtL3(dppf)]$^+$, 100%; 144.96 (144.83) PF$_6^-$, 100%. FTIR (KBr, cm^{-1}): 1591, ν(C = N); 1343, ν_s(NO$_2$); 1098, ν(N-N); 812, δ(NO$_2$ + furan); 842, ν(P-F); 558, δ(FPF); 1476, 1437, 1097, 694, 502, dppf. ^{1}H NMR [DMSO-d_6, Me$_4$Si, δ/ppm]: 8.43 [s, 1, H9], 7.94 [dd, J_1 = 7.35 Hz and J_2 = 3.02 Hz, 4, PPh$_2$], 7.75 [m, 4, PPh$_2$], 7.60 [m, 9, H2 + PPh$_2$], 7.45 [m, 4, PPh$_2$], 7.40 [d, J = 6.75 Hz, 1, H3], 7.05 [s, 1, H5], 4.75 [s, 2, H$_b$], 4.69 [s, 2, H$_c$], 4.62 [s, 2, H$_a$], 4.00 [s, 2, H$_d$], 1.11 [t, J = 6.37 Hz, 3, H11]. ^{13}C NMR [DMSO-d_6, δ/ppm]: 175.9 (C8), 142.7 (C5), 135.6 (CH, PPh$_2$), 134.9 (CH, PPh$_2$), 132.9 (C2), 130.5 (CH, PPh$_2$), 128.9 (C3), 128.8 (CH, PPh$_2$), 77.1 (C$_c$), 76.3 (C$_d$), 75.6 (C$_b$), 75.2 (C$_a$), 13.6 (C11).

[PtL4(dppf)](PF$_6$)·CH$_2$Cl$_2$, Pt-dppf-L4 Yield: 50 mg, 74%. Found: C, 44.45; H, 3.22; N, 4.36. Calc. for C$_{47}$H$_{39}$Cl$_2$F$_6$FeN$_4$O$_3$P$_3$PtS: C, 44.50; H, 3.10; N, 4.42. ESI MS *m/z*: [Calculated (Found)]: 1038.11 (1038.23) [PtL4(dppf)]$^+$, 100%; 144.96 (144.87) PF$_6^-$, 100%. FTIR (KBr, cm^{-1}): 1597, ν(C = N); 1343, ν_s(NO$_2$); 1096, ν(N-N); 812, δ(NO$_2$ + furan); 841, ν(P-F); 558, δ(FPF); 1480, 1438, 1099, 695, 496, dppf. ^{1}H NMR [DMSO-d_6, Me$_4$Si, δ/ppm]: 10.40 [s, 1, H9], 7.94 [m, 4, PPh$_2$], 7.81 [m, 4, PPh$_2$], 7.64 [m, 5, H2 + PPh$_2$], 7.54 [m, 8, PPh$_2$], 7.41 [m, 3, H3 + H$_{orto}$], 7.34 [t, J = 7.05 Hz, 2, H$_{meta}$], 7.14

[d, J = 7.37 Hz, 1, H_{para}], 7.07 [s, 1, H5], 4.73 [s, 2, H_b], 4.68 [s, 2, H_d], 4.56 [s, 2, H_c], 4.22 [s, 2, H_a]. ^{13}C NMR [DMSO-d_6, δ/ppm]: 179.1 (C8), 142.5 (C5), 135.3 (CH, PPh_2), 134.9 (CH, PPh_2), 134.3 (C2), 132.4 (CH, PPh_2), 130.0 (CH, PPh_2), 129.4 (C_{meta}), 128.8 (C3), 128.7 (C_{para}), 128.5 (C_{orto}), 77.8 (C_d), 77.7 (C_b), 75.6 (C_c), 73.9 (C_a).

DMSO solutions of all the complexes (10^{-3} M) showed molar conductivity (Λ_M) values between 22 and 28 Scm^2mol^{-1}.

X-ray diffraction study of [M(L)(dppf)](PF_6) compounds, where M = Pd(II) or Pt(II)

Single crystals suitable for structural X-ray diffraction studies of four of the compounds, namely [Pd[II](**L2**)(dppf)](PF_6), [Pt[II](**L1**)(dppf)](PF_6), [Pd[II](**L3**)(dppf)](PF_6) and [Pt[II](**L3**)(dppf)](PF_6), were obtained by slow diffusion of hexane into dichloromethane solutions of the complexes. The measurements were carried out on an Oxford Xcalibur Gemini, Eos CCD diffractometer with graphite-monochromated MoKα (λ = 0.71073 Å) radiation. X-ray diffraction intensities were collected (ω scans with ϑ and κ-offsets), integrated and scaled with CrysAlisPro suite of programs.[22] The unit cell parameters were obtained by least-squares refinement (based on the angular settings for all collected reflections with intensities larger than seven times the standard deviation of measurement errors) using CrysAlisPro. Data were corrected empirically for absorption employing the multi-scan method implemented in CrysAlisPro. The structures were solved by intrinsic phasing with SHELXT and the molecular model refined by full-matrix least-squares procedure with SHELXL of the SHELX suite of programs.[23,24]

The same space group and the close values of the cell constants indicated that [Pt(**L3**)(dppf)](PF_6) complex is isomorphic to the palladium analogue. In fact, an initial molecular model assuming the same positions of non-H atoms as in [Pd(**L3**)(dppf)](PF_6)

crystal with the identity of the metal changed to platinum lead to smooth convergence of the structural parameters for this latter compound during the least-squares refinement against the corresponding X-ray data set.

The hydrogen atoms were positioned on stereo-chemical basis and refined with the riding model. The methyl group in [Pd(**L2**)(dppf)](PF$_6$) and in the isomorphic [M(**L3**)(dppf)](PF$_6$) (M = Pd, Pt) complexes was refined as a rigid group allowed to rotate around the corresponding N-CH$_3$ or C-CH$_3$ bond such as to maximize the sum of the residual electron density at the calculated H-positions; as a result it converged to staggered angular conformation. Crystal data and structure refinement results are summarized in Table S1. Crystallographic structural data have been deposited at the Cambridge Crystallographic Data Centre (CCDC). Enquiries for data can be directed to: Cambridge Crystallographic Data Centre, 12 Union Road, Cambridge, UK, CB2 1EZ or (e-mail) deposit@ccdc.cam.ac.uk or (fax) +44 (0) 1223 336033. Any request to the Cambridge Crystallographic Data Centre for this material should quote the full literature citation and the reference numbers CCDC 1547863 [Pd(**L2**)(dppf)](PF$_6$), CCDC 1547864 [Pt(**L1**)(dppf)](PF$_6$), CCDC 1422927 [Pd(**L3**)(dppf)](PF$_6$) and CCDC 1422928 [Pt(**L3**)(dppf)](PF$_6$).

Lipophilicity studies

Reversed-phase thin layer chromatography (TLC) experiments were done on precoated TLC plates SIL RP-18W/UV$_{254}$ and eluted with MeOH:DMF:H$_2$O (65:5:30 v/v/v). Stock solutions were prepared in pure methanol (Aldrich) prior to use. The plates were developed in a closed chromatographic tank, dried and the spots were located under UV light. The R$_f$ values were averaged from two to three determinations, and converted to R_M via the relationship: $R_M = \log_{10}[(1/R_f) - 1]$.[25, 26]

Biological studies

Viability on T. cruzi (Dm28c clone) trypomastigotes. Viability assays were done by using

the MTT (3-(4,5-dimethylthiazol-2-yl)-2,5-diphenyl tetrazolium bromide) reduction method

as previously described.[27,28] Briefly, 1×10^7 trypomastigotes (see ESI for details) were

incubated in fetal bovine serum-RPMI culture medium at 37 °C for 24 h with and without the

complexes under study at different concentrations. An aliquot of the parasite suspension was

extracted and it was incubated in a flat-bottom 96-well plate and MTT was added at a final

concentration of 0.5 mg/mL, incubated at 28 °C for 4 h, and then solubilized with 10%

sodium dodecyl sulfate 0.1 mM HCl and incubated overnight. Formazan formation was

measured at 570 nm with the reference wavelength at 690 nm in a multiwell reader

(Biochrom® Asys Expert Plus, Biochrom, USA). Untreated parasites were used as negative

controls (100 % of viability). Finally, a non-linear regression analysis, using Log

concentration *vs* normalized response fit, by Graph Pad prism® software was performed.

Viability assays for T. brucei. A 200 μL cell suspension containing 5 x 10^5 parasites/mL

(bloodstream *T. b. brucei* , strain 427, cell line 449 expressing an ectopic copy of the redox

biosensor hGrx-roGFP2, see ESI for details) in exponential growth phase were seeded per

well in a 96-well culture plate and 2 μL of each compound prepared at different

concentrations in 100 % v/v DMSO were added. Control wells included cells treated with 1

% v/v DMSO or 12.5-15 μM Nifurtimox. After 24 h incubation, 100 μL from each well were

transferred to a tube containing 200 μL of sterile PBS with glucose 1 % (w/v). Prior to

analysis by flow cytometry, propidium iodide (PI) was added at a final concentration of 2

μg/mL and used as a viability marker. Samples were analyzed with a C6Accuri flow

cytometer (BD) using a 488 nm laser and the following filters λ_{em} = 530/40 nm and λ_{em} =

613/30 nm for GFP and PI signal, respectively. The data were processed and analyzed with

the C6Accuri software, where cell viability was calculated as follows: viability (%) = 100 ×

(number of cells for compound Y at concentration X/ number of cells in the DMSO-treated

control). For the selected compounds, the IC_{50} was determined using a 7-point inhibition plot

with each concentration (0.01 to 100 μM) tested in triplicate.[29,30]

Cytotoxicity on endothelial mammalian cells. Viability assays were performed on

endothelial cell lines EA.hy926 (permanent human cell line derived by fusing human

umbilical vein endothelial cells–HUVEC with human lung cells-A549, see ESI for details)

by using the MTT reduction method as previously described for *T. cruzi* trypomastigotes

assay (see above).

In vivo toxicity on zebrafish (Danio rerio) larvae. Two zebrafish adult males and females

were placed the night before spawning in breeding tanks to let them cross using glass

marbles as spawning substrate. Collected fertilized eggs were maintained in Petri dishes with

E3 embryo medium (5mM NaCl, 0.17 mM KCl, 0.33 mM $CaCl_2$, 0.33 mM Mg_2SO_4 and

0.0001 % methylene blue) at 28 °C. 72 h post fertilization, zebrafish embryos were placed in

96-well plates (3 embryos per well) containing 225 μL of E3 medium and incubated for

additional 24 h at 28°C. [Pt(**L3)**(dppf)](PF_6) was tested at 1, 10 and 100 μM concentrations

in a total 250 μL/well volume. DMSO at a 1 % final concentration was used to avoid

compound precipitation. Viability was assessed by presence of heartbeat under stereoscopic

microscope observation after 48 h treatment.

Insight into the mechanism of action

Generation of free radical species in T. cruzi. The free radical production capacity of the new complexes was assesed in the parasite using ESR (electron spin resonance) with DMPO (5,5-dimetyl-1-pirroline-*N*-oxide) for spin trapping. Each tested compound was dissolved in DMF (*N,N*-dimethylformamide, spectroscopy grade, approx. 1 mM) and the solution was added to a mixture containing the epimastigote form of *T. cruzi* (Dm28c strain; final protein concentration 4-8 mg/mL) and DMPO (final concentration, 250 mM). The mixture was transferred to a 50 μL capillary. ESR spectra were recorded in the X band (9.85 GHz) using a Bruker ECS 106 spectrometer with a rectangular cavity and 50 kHz field modulation. All spectra were registered in the same scale, after 15 scans. [31,32] The ESR spectra were simulated using the program WinSim 2002, 0.98 version.

Respiration experiments. Dm28c strain *T. cruzi* epimastigotes were harvested by $500 \times g$ centrifugation, followed by washing and re-suspension in 0.05 M sodium phosphate buffer (pH 7.4) containing 0.107 M sodium chloride. Respiration measurements were carried out polarographycally with a Clark electrode No. 5331 (Yellow Springs Instruments, 53 YSI model). [32] The chamber volume was 0.6 mL and the temperature was 28 °C. Compounds, dissolved in DMSO, were added in 40 μM final concentration. The amount of parasite used was equivalent to 1.2 mg of protein/mL. Results were corrected according to the observed effect produced by DMSO alone.

In vitro assays with recombinant redox biosensor. Recombinant hGrx-roGFP2 protein was expressed and purified as previously described, pre-reduced with DTT 20 mM in PBS containing 1 mM EDTA for 1 h at room temperature. [29,33] The excess of reducing agent was

16

removed by gel filtration on a Sephadex G25 (PD10 column, GE-Healthcare) equilibrated with PBS (pH 7.4) 1 mM EDTA. Protein concentration was measured at 280 nm, where ε_{280} = 23290 $M^{-1}cm^{-1}$ for hGrx-roGFP2. The reduced biosensor (1 µM) was treated with the different compounds added at 10 µM for 1 h at room temperature, and then the fluorescence spectra at λ_{em}= 510 nm recorded on a Cary Eclipse equipment. Controls included treatment of the biosensor with 10 µM reduced glutathione (GSH), 100 µM glutathione disulfide (GSSG) (1 h incubation) and/or 2 mM dithiotreitol (DTT) (30 min incubation) added or not of test compounds at 10 µM.

DNA interaction studies

Fluorescence experiments. Experiments for competitive binding to calf thymus DNA (CT-DNA, SIGMA, Type Y, No. D-1501) with ethidium bromide (EB, SIGMA) were carried out in 10 mM Tris-HCl buffer at pH 7.4. CT-DNA solution (1 mg/mL ~ 2 mM·nucleotide^{-1}) [34] was pre-incubated with EB (5 mM) at 4 °C for 24 h. Samples were prepared with a total concentration of DNA and EB of 20 µM·nuc^{-1} and 10 µM, respectively, varying the total complex concentration from 1-110 µM (final DMSO concentration of 5 % v/v). They were incubated at 37 °C for 30 min. Fluorescence spectra were recorded from 520 nm to 650 nm at an excitation wavelength of 510 nm on a Shimadzu RF-5301PC spectrofluorimeter. Fluorescence emission intensity was corrected for the absorption and emission inner filter effects and the mechanism involved in the fluorescence quenching process for the compounds was analysed using the Stern-Vomer equation (see ESI for detais). [35]

Circular dichroism experiments. Calf thymus DNA was purchased from Sigma (#D3664) and used as received. The CT-DNA free of protein stock solution was prepared by

dissolution in Tris-HCl buffer. [34,36] Circular dichroism studies in the UV range were done with 3 mL solutions using quartz SUPRASIL® cuvettes of 1 cm optical path. A CT-DNA solution (50-60 μM·nucleotide^{-1}) [34] was incubated with the compounds' solutions in DMSO (5 % v/v) to obtain DNA:compound molar ratio of 1:0.5 in all cases. CD spectra were collected from 240 nm to 300 nm with 5 accumulations and a scan speed of 50 nm/min. CD studies in the visible range were done with 3.5 mL solutions using quartz cuvettes of 2 cm optical path, 200 μM·nucleotide^{-1} CT-DNA concentration and 20 % v/v of DMSO in the medium (molar ratio 1:0.5). The spectra were collected from 300 nm to 600 nm, with 3 accumulations and a 200 nm/min scan speed. The CD spectra were recorded at 25°C on a Jasco J-720 spectropolarimeter with UV–vis (200–700 nm) photomultipliers (EXEL-308). For selected samples spectra were re-measured with time, to evaluate changes with time, which did not occur.

BSA interaction studies

Fluorescence experiments. The bovine serum albumin (BSA, Sigma Aldrich) stock solution was prepared by gently dissolving the protein in PBS buffer (phosphate buffer saline, 10 mM, pH 7.4).[37] The BSA concentration in PBS buffer was kept constant in all samples (1 μM), while the complex concentration was increased from 0 μM to 20 μM (final DMSO concentration of 2 % (v/v)), to obtain the desired protein/complex molar ratios (from 1:0 to 1:20). The samples were incubated at 37 °C for 24 h. The fluorescence experiments were done on a Shimadzu RF-5301PC spectrofluorimeter using a quartz cuvette of 1 cm path length. Fluorescence spectra were recorded from 300 nm to 450 nm at an excitation wavelength of 295 nm. Fluorescence spectra were corrected for the absorption and emission inner filter effects.[35] The mechanism involved in the fluorescence quenching process was

analysed using the Stern-Volmer equation and the binding parameters were obtained using the Scatchard equation.[38-40] (see ESI for details).

Circular dichroism experiments. The BSA stock solution was prepared by dissolution in PBS buffer (10 mM, pH 7.4) and the concentration of BSA was determined as previously described.[37] The circular dichroism studies were done in the visible range with 3.5 mL solutions in quartz SUPRASIL® cuvettes of 2 cm optical path. A BSA solution (100 µM) was incubated with the compounds' stock solutions in DMSO (15% v/v) to obtain BSA:complex molar ratio of 1:1 in all cases. The CD spectra were collected from 300 nm to 600 nm with 3 accumulations and a scan speed of 200 nm/min. The CD spectra were recorded at 25 °C on a Jasco J-720 spectropolarimeter with UV–vis (200–700 nm) photomultipliers (EXEL-308).

Results and discussion

Synthesis and characterization of the complexes

Eight new organometallic heterobimetallic compounds of the bioactive 5-nitrofuryl containing thiosemicarbazone ligands HL1-HL4 with the formula [M(L)(dppf)](PF$_6$), where M = Pd(II) or Pt(II), were obtained with good purities and good yields according to the proposed synthetic scheme shown in Fig. 1 and they were exhaustively characterized in the solid state and in solution.

Characterization of the complexes in the solid state

All complexes showed a similar FTIR absorption band pattern. Spectra for analogous Pd and

Pt compounds were almost identical in agreement with isostructurality observed in their

crystal structures (see below). Based on our previous experience on vibrational behavior of

H**L** ligands and their metal complexes, most relevant vibration bands were tentatively

assigned (Table S2). [41-42] Five bands corresponding to the dppf moiety were also identified as

well as the strong stretching ν(PF) and bending δ(FPF) bands of the PF_6^- counterion at

around 840 and 560 cm^{-1}.[43,44]

Crystal structure of [M(L)(dppf)](PF₆) complexes, where M = Pd(II) or Pt(II). Figures 2,

S1 and S2 show ORTEP drawings of [Pd(**L2**)(dppf)](PF$_6$), [Pt(**L1**)(dppf)](PF$_6$) and

[M(**L3**)(dppf)](PF$_6$) (M = Pt) complexes, respectively.[45] Selected bond distances and angles

around the metal center M (M = Pd and Pt) are compared in Table 1. The molecular

structures are closely related to one another with the M(II) ion at the center of a nearly square

planar P_2NS environment (*rms* deviation of atoms from the best least-squares plane less than

0.148 Å, with the metal at less than 0.104(2) Å from the plane). The metal is *cis*-coordinated

to a bis(diphenylphosphino) ferrocene moiety acting as a bidentate ligand through the

phosphorous atoms with M-P distances in the range 2.27 – 2.38 Å. The other *cis*-positions

are occupied by a thiosemicarbazone molecule also acting as a bidentate ligand through its

sulfur atom with M-S distances in the range 2.28 – 2.30 Å, and its nitrogen atom with M-N

distances in the range 2.10 – 2.15 Å (see Table 1). A similar planar coordination around

M(II) was reported for the related 1,l'-bis (dipheny1phosphino)ferrocene pyridine-2-thiolato-

1-oxide M(II) hexafluoro phosphate [M(II) = Pd, Pt] isomorphic pair of complexes, where

the thiosemicarbazone molecule is replaced by a pyridine-2-thiolato-1-oxide anion acting as

bidentate ligand through its sulfur [M-S distances of 2.293(2) Å (Pd) and 2.303(2) Å (Pt)]

and oxygen [M-O distances of 2.059(6) Å (Pd) and 2.071(4) Å (Pt)] atoms, and also for

[PdCl$_2$(dppf)] complex, where a pair of chloride ions at *cis*-positions replace the organic ligand.[17,43]

Promoted by delocalized π-bonding, the relative rotational freedom around the N-N σ-bond and the coordination to the metal, the thiosemicarbazone skeletons in [Pd(**L2**)(dppf)](PF$_6$), [Pt(**L1**)(dppf)](PF$_6$) and isomorphic [M(**L3**)(dppf)](PF$_6$) compounds (M = Pd, Pt) are nearly planar (*rms* deviation of atoms from the best least-squares plane less than of 0.159 Å).

In the dppf ligands, the coordination around iron in the ferrocene moiety shows the expected Archimedean pentagonal anti-prism conformation with the 5-membered rings staggered to each other (Fe-C bond distances in the range from 1.985(4) to 2.10(1) Å). Phosphorous-C(ph) bond distances are in the 1.80(1) -1.937(5) Å range, while P-C(*Cp*) lengths are in the range from 1.773(5) to 1.829(9) Å.
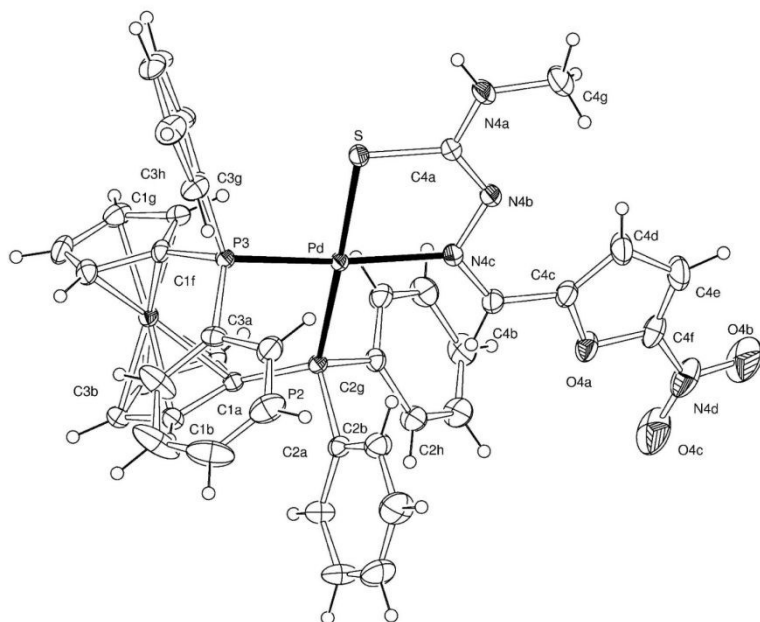

Fig. 2. View of [Pd(**L2**)(dppf)](PF$_6$) showing the non-H atoms displacement ellipsoids at the 30 % probability level. Ligand-metal interactions are indicated by full bonds. For clarity, only the thiosemicarbazone ligand is fully labeled and a few representative atoms of the bis(diphenyl1phosphino)ferrocene ligand have been labeled to indicate the numbering scheme. For the same reason, the PF$_6^-$ counter-ion was omitted.

Table 1. Bond lengths [Å] and angles [°] around the metal M in [Pd(**L2**)(dppf)](PF$_6$), [Pt(**L1**)(dppf)](PF$_6$) and isomorphic [M(**L3**)(dppf)](PF$_6$) (M = Pd, Pt) complexes.

	[Pt^{II}(L1)(dppf)](PF$_6$)	[Pd^{II}(L2)(dppf)](PF$_6$)	[Pd^{II}(L3)(dppf)](PF$_6$)	[Pt^{II}(L3)(dppf)](PF$_6$)
Selected bond lengths				
M-N(4C)	2.100 (7)	2.144 (3)	2.151 (3)	2.126 (4)
M-S	2.304 (3)	2.2841 (9)	2.282 (1)	2.293 (1)
M-P(2)	2.312 (2)	2.3688 (9)	2.378 (1)	2.339 (1)
M-P(3)	2.269 (2)	2.2785 (9)	2.275 (1)	2.263 (1)
Selected bond Angles				
N(4C)-M-P(3)	169.7 (2)	166.98 (8)	166.25 (8)	167.3 (1)
N(4C)-M-S	81.1 (2)	82.13 (8)	82.15 (8)	81.9 (1)
P(3)-M-S	89.17 (9)	87.63 (3)	87.64 (4)	88.91 (4)
N(4C)-M-P(2)	96.3 (2)	97.71 (8)	98.06 (8)	96.9 (1)
P(3)-M-P(2)	93.98 (9)	93.30 (3)	92.93 (4)	92.99 (4)
S-M-P(2)	167.1 (1)	174.03 (4)	174.86 (4)	174.61 (5)

Characterization of the complexes in solution

Molar conductivity values shown by 1 mM DMSO solutions of the complexes lie in the range reported for 1:1 electrolytes which is in agreement with the proposed formulae.[21] No conductivity changes were observed during at least 5 days at 25°C. In addition, ^{1}H NMR spectra were measured during the same period (see below); neither changes in intensity of the signals, nor new peaks due to release of free ligands were detected. Hence both data suggest that the complexes are stable in DMSO solution.

NMR results

[1]H and ^{13}C spectra were recorded in DMSO-d_6 solution. Two-dimensional NMR experiments, namely COSY and HSQC, aided in the assignment of the spectra. Results of the ^{1}H NMR experiments for the H**L** compounds and the corresponding complexes are included in Table S3. All complexes showed a similar pattern of signals corresponding to the protons

Dalton Transactions Accepted Manuscript

of **L** and dppf ligands. Integration and multiplicity were in accordance with the stoichiometry of the compounds. Even though signals appeared quite broad in some of the obtained complexes, four signals corresponding to the two H atoms of the furan ring, CH=N and NH-R protons of the thiosemicarbazone ligand were easily distinguishable. A shift of the signals of these protons in respect to the free H**L1**-H**L4** compounds was observed upon coordination. In particular, the CH=N proton (proton 5, Table S3) at around 8 ppm in the free thiosemicarbazone ligands was significantly shifted in all complexes according to the coordination of the imine nitrogen to the metal centre. This effect was more pronounced for the palladium complexation than for that of platinum. [32,46]

The non-detection of the signal corresponding to H7 in the spectra of the complexes, observed as a singlet with integration of 1 proton in the spectra of the four free HL ligands, demonstrated the deprotonation of the hydrazine nitrogen upon coordination.

Two singlets with four proton integration at 3.94 and 4.27 ppm were observed for the cyclopentadienyl *Cp* rings of the dppf free ligand. These signals have been assigned to equivalent Ha-Hd and Hb-Hc protons of both Cp rings (see figure in Table S3) that are coplanar to each other and with an average eclipsed conformation at room temperature.[47,48] A splitting of these two signals in four singlet signals that integrate for four protons was observed for all the new $[M(\mathbf{L})(dppf)](PF_6)$ compounds, with the exception of Pt-dppf-**L1** (Table S3). In this last case only 3 singlets were observed due to the overlapping of the signals of H_b and H_c (at 4.76 ppm integrating four protons). This assignment was confirmed by ^{1}H-^{1}H COSY experiments where a correlation pattern $H_a \rightarrow H_d \rightarrow H_c, H_b$ was observed. In general, the equivalence of the *Cp* protons in free dppf is broken upon formation of the M-dppf-L complexes due to the loss of fluxionality caused by the geometric requirements of the M-P bonding in the presence of the bidentate **L** ligand.[18,49,50]

Dalton Transactions Accepted Manuscript

At higher ppm values (7.45 – 7.95 ppm), multiplets corresponding to the protons of the PPh₂ units of the dppf moiety were observed.

2D-HSQC experiments allowed the assignment of the ^{13}C NMR signals (Table S4). The assignment of the carbon of thiocarbonyl group (-C=S) was performed directly in the ^{13}C-NMR spectra based on chemical shift values previously reported for other H**L** complexes.

Cyclic voltammetry studies

The electrochemical properties of the complexes were investigated by cyclic voltammetry. The eight compounds showed similar voltammetric responses in both, cathodic and anodic directions. Relevant electrochemical data obtained for the compounds are summarized in Table 2.
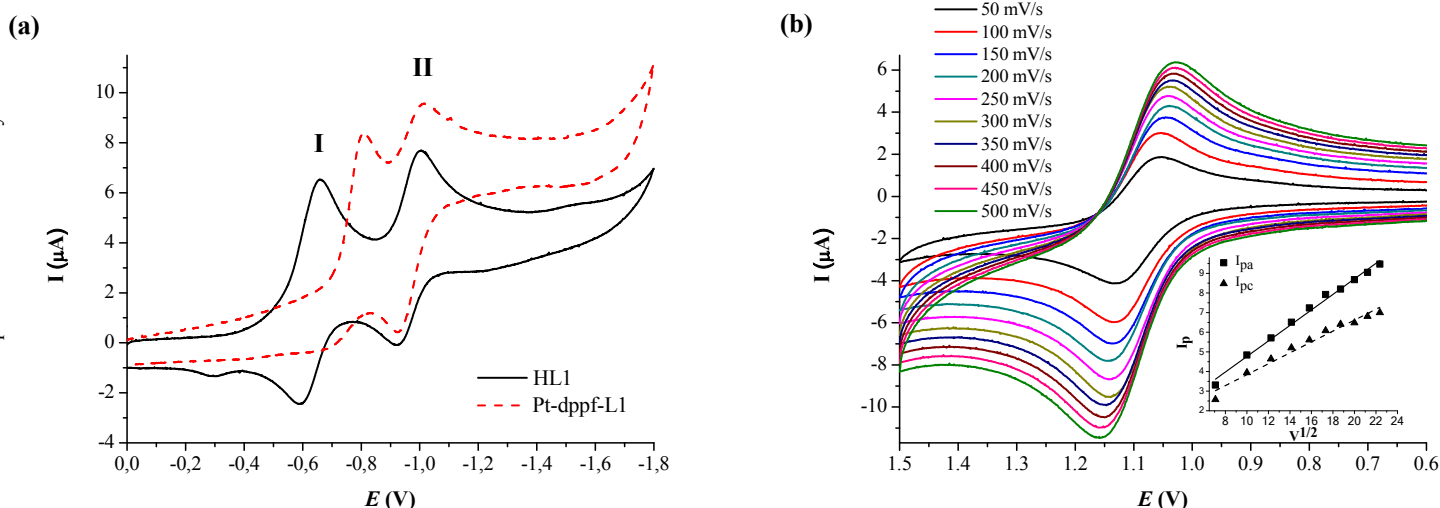
Fig. 3. (a) Cyclic voltammogram of [Pt^{II}(**L1**)(dppf)](PF₆) and of H**L1** in the cathodic direction at 100 mV/s. (b) Cyclic voltammograms of [Pt^{II}(**L1**)(dppf)](PF₆) in the anodic direction (0.6 – 1.5 V) at different scan rates. Inset: graph of Randles-Sevcik equation for the [Pt^{II}(**L1**)(dppf)](PF₆) anodic couple.[51]

Table 2. Relevant electrochemical data of the [M^{II}(**L**)(dppf)](PF₆) compounds, where M = Pd or Pt.

Compounds	Fe^{II}/Fe^{III}	Couple I (HL)		Couple II (HL)	
	$E_{1/2}$	E_{pa}	E_{pc}	E_{pa}	E_{pc}

Pd-dppf-**L1**	1.09	-0.61 (-0.92)	-0.73 (-0.80)	-0.96	-0.94 (-1.02)
Pd-dppf-**L2**	1.09	-0.60 (-0.98)	-0.70 (-0.85)	-0.91	-0.96 (-1.11)
Pd-dppf-**L3**	1.09	-0.71 (-0.95)	-0.71 (-0.84)	-0.94	-0.97 (-1.10)
Pd-dppf-**L4**	1.08	-0.55 (-0.92)	-0.65 (-0.81)	-0.94	-0.92 (-1.04)
Pt-dppf-**L1**	1.09	-0.59 (-0.92)	-0.66 (-0.80)	-0.93	-1.00 (-1.02)
Pt-dppf-**L2**	1.09	-0.60 (-0.98)	-0.67 (-0.85)	-0.97	-1.03 (-1.11)
Pt-dppf-**L3**	1.09	-0.60 (-0.95)	-0.67 (-0.84)	-0.99	-1.07 (-1.10)
Pt-dppf-**L4**	1.09	-0.52 (-0.92)	-0.61 (-0.81)	-0.82	-0.91 (-1.04)

As previously stated for the free H**L** ligands and their metal complexes, the new compounds

show a quasi reversible reduction process around -0.6 – -0.7 V (*vs.* Ag/AgCl), corresponding

to the generation of a nitro anion radical ($NO_2^{\cdot -}$) by one electron reduction of the nitro group

of the thiosemicarbazone (couple I) (Fig. 3a).[32,46] Previous cyclic voltammetry studies

demonstrated that coordination of the 5-nitrofuryl thiosemicarbazone compounds H**L** to

palladium and platinum ions lead to a displacement of the potential of the nitro group – nitro

anion radical couple to less negative values. A similar behavior was observed for this new

series of H**L** compounds (Table 2). This change could be biologically relevant, since it would

favor the generation of toxic oxygen radical species (ROS) in the parasite, initiated by

reduction of the nitro group for the {M(dppf)} H**L** compounds in respect to the free ligands

and Nifurtimox. This bioreduction could be one of the mechanisms involved in the biological

action of the new compounds against trypanosomes.[32,46]

Towards more negative potentials (around – 1.0 V) all compounds showed another quasi-

reversible electrochemical process, couple III, that was assigned to the further reduction of

the nitro group to hydroxylamine (Fig. 3a). [52,53]

In the anodic direction, a reversible redox couple characteristic of the Fe^{III}/Fe^{II} couple of the

dppf ligand was observed at around 1.09 V for all the compounds (Fig. 3b, Table 2).[18,54-56] In

all cases the anodic and cathodic peak potentials (*E*pa and *E*pc) of this couple were

independent of the scan rate (in the range 50 to 500 mV/s) and the ΔE_p values were around

59 mV (Fig. 3b). In addition, the ip/$v^{1/2}$ values did not change when modifying the scan rate,

Dalton Transactions

and the ratio of cathodic to anodic peak currents (ipc/ipa) remained close to unit. This behaviour is typical of a reversible charge transfer process.[50,57-60]

Lipophilicity

Lipophilicity is a very important physicochemical property of prospective drugs that determines biological behaviour, particularly transmembrane transport and interaction with biological receptors. Therefore, its correlation with the observed biological activity is usually a relevant characteristic to be checked.

Since the new compounds do not show adequate solubility in water to allow the determination of LogP values in the conventional way, the lipophilicity was experimentally determined using reversed-phase TLC, where the stationary phase (precoated TLC-C18 plates) may be considered to simulate lipids of biological membranes or receptors, and the mobile phase (MeOH:DMF:H_2O (65:5:30 v/v/v)) resembles the aqueous biological milieu. The composition of the mobile phase was tuned-up in order to allow differentiating complexes and free thiosemicarbazone ligands according to their lipophilicity. The most lipophilic compounds run less in this TLC system and, therefore, the method allows to compare lipophilicities of free ligands with complexes and complexes among them, all determined in the same experimental conditions.

As expected, the lipophilicity increased from the free ligand to its metal compounds due to the inclusion of the {M(dppf)} moiety and also for each series of complexes (Pt-dppf-**L** or Pd-dppf-**L**), as the *N*-substituent in the thiosemicarbazone ligand changes from hydrogen to phenyl, *i.e.* from M-dppf-**L1** to M-dppf-**L4** (Table 3, column on the right).

Results of biological studies

Anti-Trypanosoma cruzi* and anti-*Trypanosoma brucei* in vitro activities.

Results of *in vitro* activity on *T. cruzi* trypomastigotes (Dm28c) and bloodstream *T. b. brucei*

(strain 427) cell line 449 are depicted in Table 3.

Table 3. *In vitro* activity (measured as the IC_{50} value, the half inhibitory concentration) against *T. cruzi* tripomastigotes (Dm28c) and *T. brucei*, cytotoxicity on EA.hy926 endothelial cells and selectivity index (SI) values of $[M(L)(dppf)](PF_6)$ complexes and H**L1**-H**L4** (included for comparison). R_M values (lipophilicity) of the complexes and the corresponding free ligands, determined by reversed phase TLC using MeOH:DMF:H_2O (65:5:30 v/v/v) as mobile phase, are also depicted.

Compound	EA.hy926 $IC_{50}/\mu M$	*T. cruzi* $IC_{50}/\mu M$	SI [a]	*T. brucei* $IC_{50}/\mu M$	SI [b]	R_M
HL1	>100	9.8 ± 1.5[c]	>10	1.1[d]	>90	-1.0
$[Pd(\mathbf{L1})(dppf)](PF_6)$	>50	7.58 ± 0.10	>7	0.90 ± 0.05	>55	0.03
$[Pt(\mathbf{L1})(dppf)](PF_6)$	>50	3.11 ± 0.05	>16	0.77 ± 0.02	>65	-0.02
HL2	>100	17.4 ± 1.9[c]	>6	11.0[d]	>9	-0.95
$[Pd(\mathbf{L2})(dppf)](PF_6)$	>50	1.42 ± 0.02	>35	0.93 ± 0.03	>54	0.07
$[Pt(\mathbf{L2})(dppf)](PF_6)$	>50	0.79 ± 0.06	>63	0.60 ± 0.03	>83	0.10
HL3	>100	18.5 ± 1.7[c]	>5	17.0[d]	>6	-0.91
$[Pd(\mathbf{L3})(dppf)](PF_6)$	>50	3.6 ± 0.05	>14	0.98 ± 0.06	>51	0.16
$[Pt(\mathbf{L3})(dppf)](PF_6)$	>50	0.76 ± 0.03	>66	0.52 ± 0.03	>56	0.16
HL4	>100	22.7 ± 1.6[c]	>4	>100[d]	-	-0.41
$[Pd(\mathbf{L4})(dppf)](PF_6)$	>50	29.4 ± 2.03	>2	1.56 ± 0.04	>32	0.31
$[Pt(\mathbf{L4})(dppf)](PF_6)$	>50	1.32 ± 0.21	>38	1.01 ± 0.04	>50	0.35
Nifurtimox	-	20.1[e]	-	15.0[e]	-	-
Suramin	-	-	-	0.078[e]	-	-

[a]: IC_{50} EA.hy926 / IC_{50} *T. cruzi*
[b]: IC_{50} EA.hy926 / IC_{50} *T. brucei*
[c]: [42]
[d]: [61]
[e]: [29]

All compounds displayed IC_{50} values against both parasites in the low micromolar or sub-

micromolar range, with those containing platinum presenting an overall higher activity than

those with palladium (Table 3). The platinum-based H**L2** and H**L3** compounds showed the

highest anti-*T. brucei* (IC$_{50}$ = 0.60 μM and 0.52 μM, respectively) and anti-*T. cruzi* (0.79 and 0.76 μM, respectively) activities.

The new metal compounds are up to 26 times more active than the reference drug Nifurtimox on *T. cruzi* (IC$_{50}$ = 20 μM) and up to 30 times (IC$_{50}$ = 15 μM) on *T. brucei*.

Antiparasitic activity significantly increased by generation of the M-dppf-L compounds. A 3-24 fold increase and up to 99-fold increase of activity with respect to free ligand HL was observed for *T. cruzi* and *T. brucei*, respectively (Table 3).

In general, no correlation between antiparasitic activity (*T. cruzi* and *T. brucei*) and lipophilicity was observed (Table 3). In particular, the complexes containing **L4** are the more lipophilic ones but not the more active compounds. Both Pd- and Pt-**L4** compounds showed similar lipophilicity but quite different antiparasitic activity.

Unspecific cytotoxicity on mammalian cell model

Cytotoxicity was determined using EA.hy926 endothelial cells as mammalian cell model. Selectivity index values for all the complexes and free HL ligands were calculated by dividing the IC$_{50}$ on EA.hy926 cells by the IC$_{50}$ on each parasite, *T. cruzi* or *T. brucei* (Table 3).

The new metal compounds showed selectivity indexes in the range 2-66 for *T. cruzi* and 32-83 for *T. brucei*. Unspecific cytotoxicity of the H**L1**-H**L4** ligands was significantly reduced in most of the M-dppf-**L** complexes (Table 3). These 5-nitrofuryl containing thiosemicarbazone metal compounds constitute the first group of compounds that shows comparable good potencies and selectivities towards two different pathogenic trypanosomes. A similar decrease of cytotoxicity by generation of an M-dppf complex had been observed

for the previously reported pyridine-2-thiolato-1-oxide compounds in comparison with analogous Pd and Pt classical coordination compounds.[18]

In vivo toxicity

Zebrafish (*Danio rerio*) is a small cyprinid naturally found in the Ganges River in South-East Asia. Its high breeding rate (a single mature female lays 50–200 eggs per day), easy view of embryogenesis and organ development, small size, fast and external development of the embryos, availability of genomics databases and molecular tools and a relative high human-gene ontology and low cost have converted it in a major model in developmental biology and drug discovery. In particular, zebrafish is increasingly employed as toxicological model for evaluating toxicity in drug screening assays.[62] In the past, we and other researchers have successfully used this model for studying *in vivo* toxicity of new prospective metal-based drugs.[63,64]

Being [Pt(**L3**)(dppf)](PF$_6$) the most active and selective compound of the new series, its *in vivo* toxicity on zebrafish embryos was tested. All zebrafish embryos were alive in the [Pt(**L3**)(dppf)](PF$_6$) whole concentration range examined (1-100 μM) and no apparent toxicity was observed at the endpoint (48 h) of the assays.

Insights into the mechanism of action

Production of free radicals in T. cruzi

It has been shown that the principal mechanism of anti *T. cruzi* action of the 5-nitrofuryl containing thiosemicarbazone bioactive compounds involves the intraparasite bioreduction leading to toxic free radicals.[17,65] This mechanism of action is also retained by other previously reported metal complexes that include these thiosemicarbazone ligands.[32,46,66]

As previously stated, the first step of this mechanism involves the one electron reduction of the nitrofuran moiety. The cyclic voltammetry studies showed that this reduction could be more easily achieved for the M-dppf-**L** complexes than for the free thiosemicarbazone compounds, hence possibly facilitating the bioreduction mechanism. In order to assess the free radical production capacity of the new heterobimetallic compounds, ESR experiments were carried out after incubating the compounds with *T. cruzi* (Dm28c strain) epimastigotes. DMPO was added as spin trapping agent to detect free radical species having short half-time lives. All complexes showed a similar line pattern in the ESR spectra that is exemplified by the ESR spectrum obtained in the presence of $[Pd^{II}(\mathbf{L4})(dppf)](PF_6)$, displayed in Fig. S3.

In all cases, a ten line spectral pattern was observed. These lines correspond to two different DMPO spin adducts. One of these spin adducts (marked with + in Fig. S3) corresponds to the trapping of a carbon centered radical by DMPO showing the characteristic six line pattern (a_N = 16.1 G and a_H = 23.1 G).[67] This trapped species could be related to the bioreduction of the complexes, generating a nitroheterocyclic radical. The second spin adduct (*, Fig. S3) consisting of four lines of 1:2:2:1 intensities ($a_N = a_H = 14.8$ G) corresponds to DMPO-OH species. Intracellular hydroxyl radical species would arise due to intraparasite redox cycling processes.

These results confirm the biological free radical production capacity of the M-dppf-**L** complexes and their subsequent participation in redox cyclic processes generating reactive oxygen species. It can then be concluded that the complexes would maintain the mode of action of the free thiosemicarbazone ligands.

Effect on the oxygen consumption of T. cruzi

The involvement of the M-dppf-**L** complexes in redox cycling process should increase the

parasite oxygen consumption. This effect has been previously reported for the

thiosemicarbazone compounds and other complexes that include them.[32,46,65] Thus, the effect

of the obtained complexes on the oxygen uptake of *T. cruzi* epimastigotes was measured and

results are shown in Table S5.

All complexes modified oxygen uptake by the parasites, increasing oxygen consumption.

These results are in accordance with the detection of free radical species in the ESR

xperiments and therefore confirm the bioreduction of the complexes and their participation in

redox cyclic processes. However, no correlation between oxygen uptake and anti-*T. cruzi*

activity was observed indicating that other mechanisms are also involved in parasites´ death.

Redox changes in T. brucei

Ferrocenes are known to undergo one electron oxidation, which in biological systems may

lead to the formation of radicals and the concomitant oxidation of macromolecules, with the

thiol groups of proteins and low molecular metabolites (i.e. glutathione) being important

nucleophilic targets. The potential redox activity underlying the killing mechanism of

trypanosomes by ferrocene complexes was investigated using *T. brucei* parasites expressing

a redox biosensor. The biosensor (hGrx-roGFP2) is based on human glutaredoxin (hGrx)

coupled to a redox sensitive green fluorescence protein (roGFP2) that is able to translate

changes in the glutathione/glutathione disulfide (GSH/GSSG) ratio into changes in its

fluorescence intensity (*e.g.* its oxidation leads to a decrease in its fluorescence intensity at

510 nm upon excitation at 488 nm). An increase in this ratio indicates oxidation of the redox

biosensor to its disulfide form.[33] Parasites expressing the redox biosensor were incubated for

24 h with the complexes at concentrations close to or above their IC_{50} values (0.37, 1.1 and

3.30 μM). Only Pt-dppf-**L1** and Pt-dppf-**L2** added at 4- and 5-fold, respectively, of their IC_{50}

values produced almost 30 % oxidation of the biosensor, which is equivalent to the oxidation caused by 250 μM H_2O_2, under the same experimental conditions (Fig. S4).

In vitro assays performed with the recombinant biosensor and reduced glutathione, confirmed that both Pt compounds were not capable to act as direct oxidants of these molecules (Fig. S5). Taken together, these experiments clearly support that the intracellular oxidative shift triggered by Pt-dppf-**L1** and Pt-dppf-**L2** complexes is not consequence of a direct action of these compounds on the redox probe or glutathione but most likely mediated by secondary oxidative species generated by them (ROS) upon reductive activation and/or by inhibition of important components of the parasite redox system.[68]

In contrast, the Pd-dppf-**L1** complex produced a 40 % increase in fluorescence intensity of the biosensor. The physiological cause behind this phenomenon remains unknown but given the specificity of the redox biosensor for the couple GSH/GSSG [29], it may indicate a strong reductive stress exerted by Pd-dppf-**L1**.

DNA interaction studies

Fluorescence experiments

The fluorescent DNA probe, ethidium bromide (EB), was used to access the interaction of the M-dppf-**L** complexes with DNA. EB is a conjugate planar molecule with weak intrinsic fluorescence emission at the selected excitation wavelength and at pH 7.4 in Tris-HCl buffer/2 % DMSO, its spectrum shows an emission maximum at 601 nm ($\lambda_{exc.}$ = 510 nm). Intercalation of EB into double stranded DNA induces an increase of the fluorescence quantum yield.[69] In the spectrum of the {DNA-EB} adduct the emission maximum is shifted to 594 nm under these experimental conditions. Neither DNA nor the complexes are fluorescent in these experimental conditions, and no fluorescence emission results from

compounds´ direct interaction with DNA. Obtained results for the titration of the {DNA-EB}

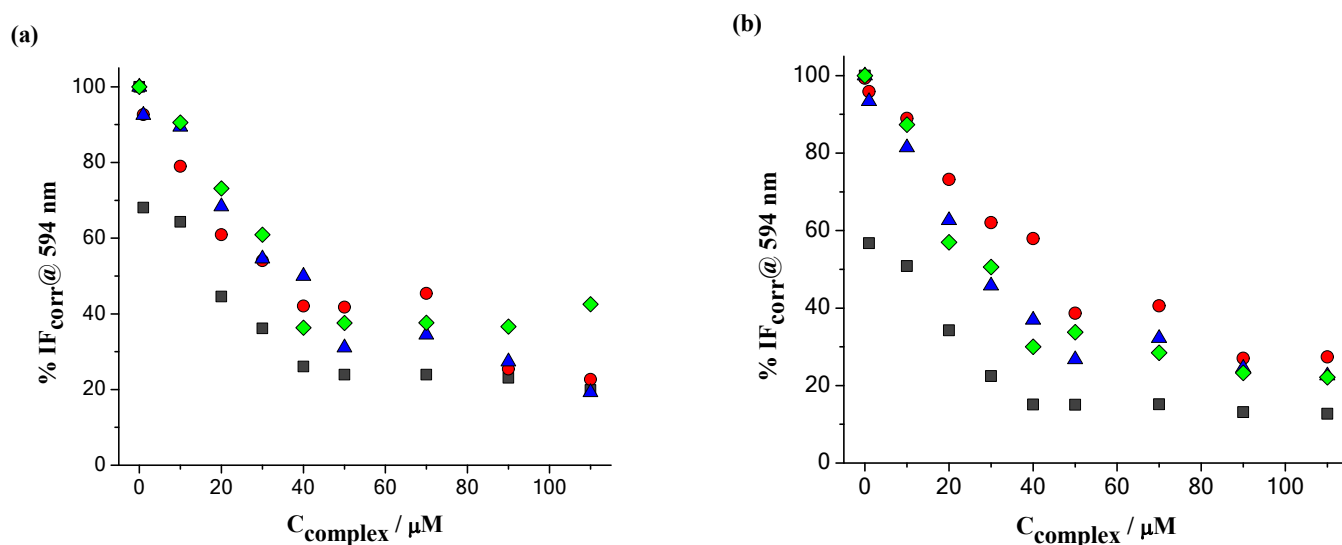adduct with the complexes are summarized in Fig. 4.

(a)

(b)

Fig. 4. Relative fluorescence intensity (%) at $\lambda_{em.}$ = 594 nm with increasing complex

concentration obtained for (a) palladium and (b) platinum complexes. (C_{DNA} = 20 µM, C_{EB} =

10 µM, samples prepared in 2% DMSO/Tris-HCl medium, 30 min incubation at 37 °C).

Squares: L1 complexes, circles: L2 complexes, triangles: L3 complexes, diamond: L4

complexes.

A quenching of the emission of {DNA-EB} adduct up to 80 % was observed upon increasing

the complexes´ concentration. The extent of the quenching was quite similar for all

complexes but those that include **L1** as ligand give rise to the highest quenching. A

bathochromic shift of 7 nm, changing the $\lambda_{max.}$ from 594 to 601 nm (characteristic of the free

EB spectrum, Fig. S6) was also observed as well as the development of two isobestic points.

These results are consistent with an EB displacement from the {DNA-EB} adduct brought

upon by the binding of the complexes to DNA in an intercalative-like manner, or by

inducing DNA conformational changes which cause the disruption of EB binding.

The fluorescence quenching process for M-dppf-**L** complexes was studied by Stern-Volmer analysis. This equation predicts a linear plot of IF_0/IF for a homogeneously emitting system. All complexes show a positive deviation from linearity at high concentration that is frequently observed when the extent of quenching is relatively large.[35] In the low concentration range of the complexes (typically up to 40 μM), the plot IF_0/IF is linear and the K_{SV} constant was calculated for each system (Table 4).

Table 4. Stern-Volmer constants obtained for $[M^{II}(\textbf{L})(dppf)](PF_6)$ compounds for the competitive binding to {DNA-EB} in 2% DMSO/Tris-HCl buffer

Compound	K_{SV} (M^{-1})	log K_{SV}
Pd-dppf-**L1**	6.6×10^4	4.8
Pd-dppf-**L2**	2.7×10^4	4.4
Pd-dppf-**L3**	2.9×10^4	4.5
Pd-dppf-**L4**	2.1×10^4	4.3
Pt-dppf-**L1**	10.1×10^4	5.0
Pt-dppf-**L2**	1.8×10^4	4.3
Pt-dppf-**L3**	4.4×10^4	4.6
Pt-dppf-**L4**	3.7×10^4	4.6

Results show that all the tested complexes interact with DNA with somewhat similar affinities. It should be stated that obtained K_{SV} values are of the same order than those previously reported for $[M^{II}Cl(L)(PTA)](PF_6)$ (M = Pd or Pt, PTA = 1,3,5-triaza-7-phosphaadamantane) complexes which showed an intercalating-like mode of DNA interaction.[70]

DNA-binding study by CD spectroscopy

Circular dichroism (CD) is a spectroscopic technique used to study systems which present intrinsic or induced chirality and may be used to assess the affinity and binding mode of small molecules, such as metal compounds, to chiral biomolecules.[71,72] DNA is a chiral molecule producing a characteristic CD spectrum in the 200-300 nm range. In particular, CT-DNA shows a typical spectrum for right-handed B form consisting of two main bands: a positive one centred at ~275 nm and a negative one at ~245 nm, due to base stacking and right-handed helicity, respectively.[73] Changes in the CD bands in this spectral range are useful to detect DNA conformational changes, damage and/or cleavage.[71,74,75] In addition, even if the complexes are not chiral and thus present no CD signal, their association with DNA may give rise to an induced circular dichroism spectra (ICD) in the range of the complexes´ absorption bands.

The conformational changes of CT-DNA induced by the M-dppf-L complexes were monitored by CD spectroscopy. As DMSO was used as solvent to allow dissolving suitable amounts of the complexes, the CD spectra could only be measured in the UV range between 240-300 nm (Fig. S7). CD spectra were also measured between 300-600 nm, where DNA has no CD bands (Fig. S8).

Upon mixing DNA with the complexes, changes in the CD spectra were immediately observed in the range 240-300 nm, with all complexes inducing a decrease in the positive band of the CD spectrum of DNA (Figures S9-S12). These results suggest that the complexes interact with CT-DNA inducing conformational changes in its structure. The complexes that include the **L1** ligand showed the greatest effect on this band.

These results are in accordance with those observed by fluorescence experiments, where the highest quenching effects were also found for the complexes containing **L1**. M-dppf-**L1** complexes having the smallest substituents in the terminal amine group possibly penetrate

Dalton Transactions Accepted Manuscript

more easily the biomolecule affecting, for example, base stacking and generating

conformational changes on DNA. It is also plausible that the presence of $-NH_2$ moiety

instead of $-NHR$ (R = Me, Et or Ph) allows establishing stronger hydrogen bonds with

suitable groups of DNA, such as phosphates.

In the CD spectra measured in the visible range, two negative bands at ~330 nm and ~450

nm were observed. The presence of these bands corresponds to induced chirality in bands of

the metal complexes, probably due to the formation of adducts between DNA and the

complexes.[72,76] In fact, the absorption spectra of the complexes, measured in similar

conditions (5 % DMSO in Tris-HCl buffer), depict two reasonably strong absorption bands at

similar wavelength values. As the extinction coefficients of bands with λ_{max} in the 425-450

nm range of the Pd- and Pt-dppf-**L** complexes are similar for all complexes (*ca.*: $1.2\text{-}1.4 \times 10^4$

$M^{-1}\,cm^{-1}$), the intensity of the observed induced CD (ICD) bands show that the complexes

that include the **L2** ligand either have the strongest interaction with the DNA, or bind to CT-

DNA closer to its chiral moieties.

Even though results show that DNA may be a target of these complexes, no correlation

between the interaction with this biomolecule and the biological activity was observed.

Interaction with BSA

Fluorescence experiments.

Albumin is the most abundant plasma protein and one of its principal functions is the

transport of drugs, metal ions and/or metal complexes through the blood-stream towards cells

and tissues. Bovine serum albumin (BSA) is the most commonly used homologue for human

serum albumin, and the most important protein present in cell culture media used in *in vitro*

experiments with mammalian cells, due to the addition of fetal bovine serum (FBS). It

exhibits intrinsic fluorescence emission due to the presence of phenylalanine, tyrosine and

tryptophan (Trp) residues. Among them, Trp is the dominant intrinsic fluorophore and it can

be selectively excited at $\lambda_{exc.}$ = 295 nm. BSA contains two Trp residues: Trp134 that is

located in the proximity of the protein surface and is buried in a hydrophobic pocket of

domain I and Trp 213 that is located in a hydrophobic binding pocket of subdomain IIA. In

particular Trp213 is the most sensitive to the local environment and its fluorescence emission

easily responds to small changes in the vicinity of the indole ring that may occur in response

to binding to the protein.[35] Based on this, the interaction of BSA with the

$[Pd^{II}(\textbf{L3})(dppf)](PF_6)$ complex was studied using fluorescence spectroscopy. Emission

spectra obtained through titration of BSA with the selected complex are displayed in Fig.

S13.

The studied complex generated quenching of the fluorescence emission of BSA up to 70 %

upon increasing its concentration. In addition, the complex induced a red-shift in the

emission maximum of *ca.* 4 nm. These results indicate that hydrophobicity increased around

the Trp213 environment due to the interaction between the protein and the complex.[35]

The quenching process was analysed according to Stern-Volmer equation and the binding

constant (K_{bc}) and the number of binding site types (n) were calculated from the Scatchard

equation. The obtained value of K_{SV} was 5.4×10^4 M^{-1} indicating a good BSA fluorescence

quenching ability for the compound. This K_{SV} value is similar to those previously reported

for other palladium and platinum complexes that interact efficiently with the protein.[77] The

determined binding constant was $K_{bc} = 6.1 \times 10^3$ M^{-1}, which is somewhat lower than those

reported for other metal complexes that interact reversibly with this protein (K_{bc} in the order

of 10^5 M^{-1}).[77-79] So, the obtained K_{bc} value is within a nearly optimal range: it is high enough

for the compounds to bind albumin to be transported but, nevertheless it is sufficiently low to

let the compound be released from albumin upon arrival to the target.[80] The n value obtained

was approximately equal to 1 suggesting the existence of a single binding site type between BSA and the M-dppf-**L3** complex.

Circular dichroism experiments

CD spectroscopy is a technique frequently used to monitor protein drug interactions by following e.g. changes on the protein CD spectrum. The CD spectrum in the 200–250 nm range can yield information on the secondary structure of the protein and on the changes it undergoes upon the binding of a compound. However, in the performed experiments, the need to use DMSO to solubilise the complexes precluded the use of CD spectroscopy below 300 nm (due to the DMSO cut-off absorption). In these cases CD can still be a very informative technique if ICD bands are observed. The M-dppf-**L** complexes are CD silent species, however they have absorption bands for $\lambda > 300$ nm, where BSA does not absorb radiation. Therefore, the interaction with BSA can be monitored by the development of ICD bands measured above 300 nm, which provide information only on the protein-complex bound species that can be formed in solution. Fig. S14 depicts CD spectra of solutions containing BSA and the Pd- and Pd-dppf-**L** complexes measured at 35°C, immediately after their addition to a solution containing BSA.

Binding of M-dppf-**L** complexes to BSA was detected immediately after mixing through the development of two main ICD bands. These bands were observed at ~330 nm and ~430 nm, in the same wavelength range where the complexes have absorption bands, indicating a fast interaction between BSA and the complexes. This interaction proceeds faster than that observed for previously studied $[Ru_2(p\text{-cym})_2(L)_2]X_2$ complexes (where X = Cl$^-$, PF$_6^-$; L = 5-nitrofuryl containing thiosemicarbazone ligands) which, using human serum albumin, presented ICD bands only after 1 h of incubation.[81]

Conclusions

Eight new Pd(II) and Pt(II) heterobimetallic [M(**L**)(dppf)](PF$_6$) complexes including a ferrocenyl moiety were synthesized and fully characterized. The compounds were rationally designed by including 5-nitrofuryl containing thiosemicarbazones H**L1**-H**L4** as bioactive ligands and a lipophilic and non-toxic ferrocenyl derivative as co-ligand. For the first time almost the whole series showed activity in the low micromolar or submicromolar range on both parasites and lower toxicity on mammalian cells, as well as higher selectivity towards both parasites than the free H**L1**-H**L4** ligands and the several groups of H**L** classical coordination complexes and organometallic compounds previously developed by our group. In addition, the *in vivo* test on zebrafish carried out with the most active compound of the series showed no toxicity upon 48 h contact, even for concentrations of 100 μM.

Our data confirmed the biological free radical production capacity of the obtained M-dppf-**L** complexes and subsequent participation in redox processes generating reactive oxygen species. Interestingly, the generation of intracellular redox stress in the infective form of African trypanosomes was compound specific, suggesting a selective molecular target(s) and/or activation pathway for the M-dppf-**L** complexes. As our CD (and fluorescence) measurements indicate that the compounds bind DNA, if the complexes manage to reach this biomolecule in the parasite this may also contribute to the toxicity.

Measurement of circular dichroism spectra also confirmed the binding of the reported M-dppf-**L** complexes to BSA. From fluorescence emission quenching obtained with solutions of BSA incubated with increasing concentrations of [Pd^{II}(**L3**)(dppf)](PF$_6$) a binding constant of *ca.* 6×10^3 was obtained. This is within the range suitable for being transported in blood by albumin, but low enough to let the compound be released upon contact with the target.

Globally these results show that most of these new complexes are promising antiparasitic

compounds that deserve further studies in the search for prospective broad spectrum

antitrypanosomal drugs.

Conflicts of interest

There are no conflicts of interest to declare.

Acknowledgements

References

(1) http://www.who.int/topics/tropical_diseases/en/. visited 2019.

(2) http://www.who.int/neglected_diseases/diseases/en/. visited 2019.

(3) N. M. El-Sayed *et al.*, *Science* 2005, **309**, 404–409.

(4) http://www.who.int/chagas/en/. visited 2019.

(5) M. Leslie, *Science* 2011, **333**, 934.

(6) C.J. Perez, A.J. Lymbery, R.C.A. Thompson, *Trends Parasitol.* 2015, **31**, 595-603.

(7) http://www.who.int/trypanosomiasis_african/. visited 2019.

(8) M. Berninger, I. Schmidt, A. Ponte-Sucre, U. Holzgrabe, *MedChemComm* 2017, **8**, 1872–1890.

(9) D. Gambino, L. Otero, *Inorg. Chim. Acta* 2018, **472**, 58-75.

(10) D. Gambino, *Coord. Chem. Rev.* 2011, **255**, 2193–2203.

(11) J. Costa Pessoa, S. Etcheverry, D. Gambino, *Coord. Chem. Rev*. 2015, **301-302**, 24-48.

(12) K. Kowalski, *Coord. Chem. Rev.* 2018, **366**, 91–108.

(13) D. R. van Staveren, N. Metzler-Nolte, *Chem. Rev.* 2004, **104**, 5931-5985.

(14) Y. Ching Ong, S. Roy, P. C. Andrews, G. Gasser, *Chem. Rev.* 2019, 119, 730−796.

(15) P. V. Simpson, C. Nagel, H. Bruhn, Ulrich Schatzschneider, *Organometallics*, 2015, **34**, 3809–3815.

(16) K. Kowalski, Ł. Szczupak, S. Saloman, D. Steverding, A. Jabłoński, V. Vrček, A. Hildebrandt, H. Lang, A. Rybarczyk-Pirek, *ChemPlusChem* 2017, **82**, 303-314.

(17) G. Aguirre, L. Boiani, H. Cerecetto, M. González, A. Denicola, L. Otero, D. Gambino, C. Rigol, C. Olea-Azar, M. Fagundez, *Bioorg Med Chem.* 2004, **12**, 4885-4893.

(18) E. Rodríguez Arce, M. F. Mosquillo, L. Pérez-Díaz, G. A. Echeverría, O. E. Piro, A. Merlino, L. Coitiño, C. Maríngolo Ribeiro, C. Q. F. Leite, F. R. Pavan, L. Otero, D. Gambino, *Dalton Trans.* 2015, **44**, 14453-14464.

(19) M. Fanelli, M. Formica, V. Fusi, L. Giorgi, M. Micheloni, P. Paoli, *Coord. Chem. Rev.* 2016, **310**, 41–79.

(20) T.A.K. Al-Allaf, H. Schmidt, K. Merzweiler, C. Wagner, D. Steinborn, *J. Organometal. Chem.* 2003, **678**, 48 - 55.

(21) W. J. Geary, *Coord. Chem. Rev.* 1971, **7**, 81-91.

(22) CrysAlisPro, Oxford Diffraction Ltd., version 1.171.33.48 (release 15-09-2009 CrysAlis171.NET).

(23) G. M. Sheldrick, *Acta Crystallogr.* 2015, **A71**, 3–8.

Dalton Transactions Accepted Manuscript

(24) G. M. Sheldrick, *Acta Crystallogr.* 2008, **A64**, 112-122.

(25) C. Hansch, A. Leo, The hydrophobic parameter: measurement and calculation; In Exploring QSAR. Fundamentals and Applications in Chemistry and Biology, American Chemical Society Ed., Washington, 1995, pp 97–124.

(26) H. Cerecetto, R. Di Maio, M. González, M. Risso, P. Saenz, G. Seoane, A. Denicola, G. Peluffo, C. Quijano, C. Olea-Azar, *J. Med. Chem.* 1999, **42**, 1941-1950.

(27) S. Muelas-Serrano, J. J. Nogal-Ruiz, A. Gómez-Barrio, *Parasitol. Res.* 2002, **86**, 999 - 1002.

(28) M. Faundez, L. Pino, P. Letelier, C. Ortiz, R. López, C. Seguel, J. Ferreira, M. Pavani, A. Morello, J. D. Maya, *Antimicrob. Agents Chemother.* 2005, **49**, 126-130.

(29) J. Franco, F. Sardi, L. Szilágyi, K.E. Kövér, K. Fehér, M. A. Comini. *Int. J. Parasitol. Drugs Drug Resist.* 2017, **7**, 303-313.

(30) F. Maiwald, D. Benítez, D. Charquero, M. Abad Dar, H. Erdmann, L. Preu, O. Koch, C. Hoelscher, N. Loaec, L. Meijer, M.A. Comini, C. Kunick, *Eur. J. Med. Chem.* 2014, **83**, 274-283.

(31) M.I. Bruce, N.J. Windsor, *Aust. J. Chem.* 1977, **30**, 1601–1604.

(32) L. Otero, M. Vieites, L. Boiani, A. Denicola, C. Rigol, L. Opazo, C. Olea-Azar, J.D. Maya, A. Morello, L. Krauth-Siegel, O.E. Piro, E. Castellano, M. González, D. Gambino, H. Cerecetto, *J. Med. Chem.* 2006, **49**, 3322–3331.

(33) Gutscher, A.L. Pauleau, L. Marty, T. Brach, G.H. Wabnitz, Y. Samstag, A.J. Meyer, T.P. Dick, T.P. *Nature Methods* 2008, **5**, 553-559.

(34) J.K. Barton, J.M. Goldberg, Ch. V. Kumar, N.J. Turro, *J. Am. Chem. Soc.* 1986, **108**, 2081-2088.

(35) J.R. Lakowicz, in Principles of Fluorescence Spectroscopy, Springer Science, New York, 3rd. edition, 2006, chapter 8.

(36) C. Acilan, B. Cevatemre, Z. Adiguzel, D. Karakas, E. Ulukaya, N.Ribeiro, I. Correia, J. Costa Pessoa, *Biochim. Biophys. Acta* 2017, **1861**, 218-234.

(37) T. Peters Jr., *All about Albumin: Biochemistry, Genetics, and Medical Applications*, Academic Press, New York, 1996.

(38) P. Krishnamoorthy, P. Sathyadevi, A. H. Cowley, R. R. Butorac, N. Dharmaraj, *Eur. J. Med. Chem.* 2011, **46**, 3376-3378.

(39) T.S. Singh, S. Mitra, *Spectrochim. Acta. A. Mol. Biomol. Spectrosc.* 2011, **78**, 942–948.

(40) J. Tian, J. Liu, J. Zhang, Z. Hu, X. Chen, *Chem. Pharm. Bull.* 2003, **51**, 579–582.

 (41) D. Gambino, L. Otero, M. Vieites, M. Boiani, M. Gonzalez, E. J. Baran, H. Cerecetto, *Spectrochim. Acta Part A* 2007, **68**, 341–348.

(42) E. Rodríguez Arce, I. Machado, B. Rodríguez, M. Lapier, M. C. Zúñiga, J. D. Maya, C. Olea Azar, L. Otero, D. Gambino, *J. Inorg. Biochem.* 2017, **170**, 125-133.

(43) T. Hayashi, M. Konishi, Y. Kobori, M. Kumada, T. Higuchi, K. Hirotsu, *J. Am. Chem. Soc.* 1984, **106**, 158-163.

(44) A.M. Heyns, *Spectrochim. Acta* 1977, **33**, 315-322.

(45) L. J. Farrugia, *J. Appl. Cryst.* 1997, **30**, 565.

(46) M. Vieites, L. Otero, D. Santos, C. Olea-Azar, E. Norambuena, G. Aguirre, H. Cerecetto, M. González, U. Kemmerling, A. Morello, J.D. Maya, D. Gambino, *J. Inorg. Biochem.* 2009, **103**, 411–418.

(47) A. Togni, T. Hayashi "Ferrocenes: Homogeneous Catalysis, Organic Synthesis, Materials Science" Weinheim - New York Basel - Cambridge. Tokyo, 1995.

(48) P. Stepnicka "Ferrocenes: Ligands, Materials and Biomolecules" John Wiley & Sons, England 2008.

(49) C. E. Housecroft, S. M. Owen, P. R. Raithby, B. A. M. Shaykh, *Organometallics* 1990, **9**,1617- 1623.

(50) D. Cauzzi, C. Graiff,C. Massera,G. Predieri, A. Tiripicchio, D. Acquotti, *J. Chem. Soc. Dalton Trans*. 1999, 3515–3521.

(51) P.T. Kissinger, W.R. Heineman, *J. Chem. Ed.* 1983, **60**, 702-706.

(52) C. Olea-Azar, C. Rigol, F. Mendizabal, A. Morello, J. Diego Maya, C. Moncada, E. Cabrera, R. di Maio, M. González, H. Cerecetto, *Free Radic. Res*. 2003, 37, 993–1001.

(53) C. Rigol, C. Olea-Azar, F. Mendizábal, L. Otero, D. Gambino, M. González, H. Cerecetto, *Spectrochim. Acta. A. Mol. Biomol. Spectrosc.* 2005, **61**, 2933–2938.

(54) B. Corain, B. Longato, G. Favero, D. Ajò, G. Pilloni, U. Russo, F.R. Kreissl, *Inorg. Chim. Acta* 1989, **157**, 259–266.

(55) T.M. Miller, K.J. Ahmed, M.S. Wrighton, *Inorg. Chem.* 1989, **28**, 2347–2355.

(56) P. Appelt, J.P. da Silva, O. Fuganti, L.E.N. Aquino, B. Sandrino, K. Wohnrath, V.A.Q. Santos, M.A.A. Cunha, A. Veiga, F.S. Murakami, D.F. Back, M.P. de Araujo, *J. Organomet. Chem.* 2017, **846**, 326–334.

(57) E.R. Brown, R.F. Large (1971) In: Weisberger A, Rositer BW (eds) Part IIA, Chapter 6. Interscience, New York.

(58) X. Wu, E.R.T. Tiekink, I. Kostetski, N. Kocherginsky, A.L.C. Tan, S.B. Khoo, P. Wilairat, M.-L. Go, *Eur. J. Pharm. Sci.* 2006, **27**, 175–187.

(59) M. Hocek, P. Štěpnička, J. Ludvík, I. Císařová, I. Votruba, D. Řeha, P. Hobza, *Chem. Eur. J.* 2004, **10**, 2058–2066.

(60) E.H. Kerns, L. Di, Drug-like properties: Concepts, structure design and methods from ADME to toxicity optimization. Academic Press, Amsterdam, 2008.

(61) B. Demoro, C. Sarniguet, R. Sánchez-Delgado, M. Rossi, D. Liebowitz, F. Caruso, C. Olea-Azar, V. Moreno, A. Medeiros, M. Comini, L. Otero, D. Gambino, *Dalton Trans.* 2012, **41**, 1534–1543.

(62) D. Bichara, N. B. Calcaterra, S. Arranz, P. Armas, S. H. Simonetta, *J. Appl. Toxicol.* 2014, **34**, 214–219.

(63) I. E. León, A. L. Di Virgilio, D. A. Barrio, G. Arrambide, D. Gambino, S. B. Etcheverry, *Metallomics* 2012, **4**, 1287-1296.

(64) A. J. Hill, H. Teraoka, W. Heideman, R. E. Peterson, *Toxicol. Sciences*, 2005, **86**, 6–19.

(65) L. Otero, J.D. Maya, A. Morello, C. Rigol, G. Barriga, J. Rodriguez, C. Folch, E. Norambuena, M. González, C. Olea-Azar, H. Cerecetto, D. Gambino, *Med. Chem*. 2008, **4**, 11–17.

(66) L. Otero, C. Folch, G. Barriga, C. Rigol, L. Opazo, M. Vieites, D. Gambino, H. Cerecetto, E. Norambuena, C. Olea-Azar, *Spectrochim. Acta A* 2008, **70**, 519–523.

(67) K. Makino, T. Hagiwara, A. Murakami, *Radiat. Phys. Chem*. 1991, **37**, 657–665.

(68) M. A. Comini, L. Flohé, In: Jäger, T., Koch, O., Flohé, L., editors. Trypanosomatid diseases. Weinheim: Wiley-Blackwell; 2013. p. 167–199.

(69) M.J. Waring, *J. Mol. Biol*. 1965, **13**, 269–282. C. Tan, J. Liu, L.M. Chen, S. Shi, L.N. Ji, *J. Inorg. Biochem*. 2008, **102**, 1644–1653.

(70) M. Cipriani, J. Toloza, L. Bradford, E. Putzu, M. Vieites, E. Curbelo, A.I. Tomaz, B. Garat, J. Guerrero, J.S. Gancheff, J.D. Maya, C. Olea Azar, D. Gambino, L. Otero, *Eur. J. Inorg. Chem*. 2014, **27**, 4677–4689.

(71) N.C. Garbett, P.A. Ragazzon, J.B. Chaires, *Nat. Protoc*. 2007, **2**, 3166–3172.

(72) J. Costa Pessoa, I. Correia, G. Gonçalves, I. Tomaz, *J. Arg. Chem. Soc*. 2009, **97**, 151-165.

(73) V. I. Ivanov, L. E. Minchenkova, A. K. Schyolkina, A. I. Poletayev, *Biopolymers* 1973, **12**, 89-110.

(74) I. Correia, S. Roy, C. P. Matos, S. Borovic, N. Butenko, I. Cavaco, F. Marques, A. Lorenzo, A. Rodríguez, V. Moreno, J. Costa Pessoa. S.C. Zhang, Y.G. Zhu, C. Tu, H.Y. Wei, Z. Yang, L.P. Lin, J. Ding, J.F. Zhang, Z.J. Guo, *J. Inorg. Biochem*. 2004, **98**, 2099–2106.

(75) R.F. Vitor, I. Correia, M. Videira, F. Marques, A. Paulo, J. Costa Pessoa, G. Viola, G.G. Martins, I. Santos, *ChemBioChem* 2008, **9**, 131–142.

(76) R. F. Pasternack, E. J. Gibbs, J. J. Villafrancas, *Biochemistry* 1983, **22**, 2406-2414.

(77) D. Ćoćić, S. Jovanović, S. Radisavljević, J. Korzekwa, A. Scheurer, R. Puchta, D. Baskić, D. Todorović, S. Popović, S. Matić, B. Petrović. *J. Inorg. Biochem.* 2018, **189**, 91-102.

(78) P. S. Bangde, D. S. Prajapati, P. P. Dandekar, A. R. Kapdi, *ChemistrySelect*. 2018, **3**, 5709 – 5716.

(79) G. Psomas, D. P. Kessissoglou. *Dalton Trans*. 2013, 42, 6252.

(80) J. Kljun, I. Bratsos, E. Alessio, G. Psomas, U. Repnik, M. Butinar, B. Turk, I. Turel, *Inorg. Chem*. 2013, **52**, 9039–9052.

(81) B. Demoro, M. Rossi, F. Caruso, D. Liebowitz, C. Olea-Azar, U. Kemmerling, J.D. Maya, H. Guiset, V. Moreno, C. Pizzo, G. Mahler, L. Otero, D. Gambino, *Biol. Trace Elem. Res*. 2013, **153**, 371–381.

Dalton Transactions Accepted Manuscript

New heterobimetallic palladium and platinum ferrocenyl derivatives showed submicromolar activities on both *T. cruzi* and *T. brucei* parasites and high selectivities.

Dalton Transactions Accepted Manuscript